Vasyukova, O.V., Williams-Jones, A.E., 2019. Closed system fluid-mineral-mediated trace element behaviour in peralkaline rare metal pegmatites: Evidence from Strange Lake. Chemical Geology, 505: 86-99.

Closed system fluid-mineral-mediated trace element behaviour in peralkaline rare metal pegmatites: Evidence from Strange Lake.

O.V. Vasyukova and A.E. Williams-Jones

Department of Earth and Planetary Sciences, McGill University, 3450 University Street, Montréal, Québec, Canada, H3A 0E8, olga.vasyukova@mcgill.ca

Abstract

Large peralkaline complexes are 'factories' that have produced a variety of 'exotic' minerals including high field strength element minerals. In most cases, these minerals are secondary and crystallise in a hydrothermal paragenesis that is extremely difficult to decipher due to the complexity of the textural relationships. The Strange Lake pluton is one of these complexes, and contains 37 exotic minerals, most of which are secondary. Adding to the difficulty in establishing a comprehensive paragenesis for these minerals and an alteration/precipitation path for the pluton is the fact that there were several stages of crystallisation of the same exotic and common secondary minerals, e.g., bastnäsite, fluocerite, gadolinite, aegirine, fluorite, and zircon.

In this paper, we present a model, which describes a detailed path for the alteration and precipitation of minerals in the closed hydrothermal system of a peralkaline granitic pegmatite, based on direct measurements of the evolving composition of the aqueous fluid that exsolved from the late-stage magma crystallising rare-metal pegmatites in the Strange Lake pluton. The driving force for this evolution was cooling-induced oxidation that ultimately transformed the CH_4-H_2 gas in this fluid to CO_2. This lead to a large drop in the pH, which was a major control on the composition of the fluid and the crystallisation of secondary minerals.

Although large numbers of minerals formed and were replaced during the different stages of fluid evolution, the changing chemistry of the fluid was largely a response to the alteration of four minerals, namely arfvedsonite, elpidite, narsarsukite and fluorite. The earliest stage of alteration, which took place at ~360 ^oC, was marked by the replacement of arfvedsonite by aegirine. This alteration decreased salinity and released K, Li, and Rb to the fluid, causing K-metasomatism. At ~ 300 ^oC, CH_4 and higher hydrocarbons reacted to produce CO_2. This caused a massive drop in pH from a value > 10 to a value of ~ 3 and intense alteration, which included the dissolution of fluorite, the breakdown of elpidite to zircon and quartz and the replacement of

narsarsukite by titanite. With ongoing dissolution of fluorite, Ca activity reached a level sufficient to promote the alteration of elpidite to armstrongite or gittinsite. This was accompanied by alteration of arfvedsonite to ferroceladonite and microcline to Al-phyllosilicates, enriching the fluid in Na, Fe and F. Soon after, there was a near total loss of CO_2 (at ~ 230 ºC). This loss was catastrophic and was focused along conical fractures (these developed as a result of the collapse of the roof of the pluton), with resultant fragmentation of the rocks along the fluid path. Alteration to phyllosilicates continued after the loss of CO_2, as the system cooled to ~ 190 ºC. This marked the beginning of the final stage of alteration, which involved the replacement of arfvedsonite by aegirine and hematite. It also coincided with large scale hematisation within the pluton. Finally, it lead to the cementation of the fragments along the fluid path to form the fluorite-hematite ring breccia that is now evident at the margins of the pluton.

The model of fluid evolution presented here is potentially applicable to many other peralkaline complexes. The only requirements are that the system was closed until a relatively late stage and that the exsolved fluid was saline and contained a reduced carbonic component. This is a feature of many peralkaline complexes, most notably, the Khibiny and Lovozero complexes in Russia, and Ilímaussaq in Greenland.

Keywords

Peralkaline granite, pegmatite, fluid evolution, closed system, coupled oxidation/acidification, HFSE mineralisation

Introduction

Peralkaline plutonic complexes (both saturated and undersaturated in terms of quartz) are characterised by the presence of an unusually large number of uncommon (exotic) minerals, including high field strength element (HFSE) minerals. Several of the best-known peralkaline complexes are the type localities for many of these minerals. For example, Mont Saint-Hilaire (Canada) is the type locality for 65 minerals (www.mindat.org). In the case of the Khibiny complex (Russia) and the adjacent Lovozero massif the numbers are 121 and 106, respectively (www.mindat.org). Other well-known alkaline plutons, such as Ilímaussaq (Greenland) and Dara-i-Pioz (Tajikistan), also are the type localities for a large number of exotic minerals (36 and 38, respectively). Most of the exotic minerals in peralkaline complexes are of late magmatic or hydrothermal origin, occurring in pegmatites, veins and miarolitic cavities, indicating the important role that fluids play in the generation of such mineralogical complexity. Not

surprisingly, therefore, intense hydrothermal alteration is reported to be a defining characteristic of many peralkaline complexes (Salvi et al., 2000; Salvi and Williams-Jones, 2005; Gysi et al., 2016; Marks and Markl, 2017), one that is manifested by the large numbers of secondary (hydrothermal) exotic minerals (greatly in excess of the number of primary magmatic minerals) in these complexes. The secondary minerals form in response to continuously changing fluid properties, such as pH, ligand distribution, as well as temperature, pressure and oxygen fugacity. As a result, the textural relationships among these minerals are so complex that in most cases it is impossible to reconstruct the crystallisation/alteration sequence.

The Strange Lake pluton (Canada), which is the subject of this paper, is arguably the best-known peralkaline granite, and is conspicuous for its large number of exotic secondary HSFE minerals It is also important as the host of a potentially economic resource of the REE, Zr and Nb. Most significantly, however, from the perspective of the subject considered here, Strange Lake is an example of a peralkaline igneous system, in which late hydrothermal alteration created numerous secondary HFSE-rich minerals and removed most of the textural evidence for the crystallisation of earlier minerals (Salvi and Williams-Jones, 1996; 2006; Gysi and Williams-Jones, 2013; Gysi et al., 2016; Vasyukova and Williams-Jones, 2018). The Strange Lake granites and pegmatites contain about 50 minerals, and for two of them it is the type locality, i.e., for gagarinite-(Ce) and gerenite-(Y) (www.mindat.org). Moreover, several of the minerals crystallised in multiple generations, e.g., aegirine (Vasyukova and Williams-Jones, 2018), and zircon and gadolinite (Gysi et al., 2016). Based on field evidence and thermodynamic modelling (Gysi and Williams-Jones, 2013), Gysi et al. (2016) developed a system of geochemical vectors designed to distinguish the different types of alteration experienced by the rocks. However, even using these vectors, it is difficult to relate the minerals to particular stages of alteration and even determine the order of these alteration stages.

In this paper, we build on our previous study of the physico-chemical properties of the evolving fluid (Vasyukova et al., 2016) and the progressive evolution of its rare earth element (REE) composition (Vasyukova and Williams-Jones, 2018). Using the data reported in these papers and new data on trace elements (other than the rare earth elements), we have reconstructed the sequence of alteration and precipitation steps for the major minerals and all the HFSE-rich minerals (including those that are REE-bearing) in the Strange Lake pegmatites during the different stages of evolution of the system. On the basis of this reconstruction, we have also evaluated the factors controlling the stability of the primary magmatic phases and the secondary minerals that crystallised during the subsequent closed-system alteration. To our knowledge, this

paper is the first dealing with rare metal pegmatites that provides a detailed reconstruction of the progressive interaction of a magmatic-hydrothermal fluid with its host, and the first to present a comprehensive model of hydrothermal alteration that will be applicable to other peralkaline igneous systems.

Geological setting

The peralkaline Strange Lake pluton is Mid-Proterozoic in age, i.e., 1240 ± 2 Ma (Miller et al., 1997), and comprises two principal granitic units and two pegmatitic fields (Fig. 1). The granites, namely hypersolvus granite and transsolvus granite, are distinguished on the basis of feldspar mineralogy (Nassif, 1993) and arfvedsonite morphology (Siegel et al., 2017). The earliest and least evolved hypersolvus granite occupies the central part of the intrusion, and is characterised by the presence of perthite, as the only feldspar, and interstitial arfvedsonite (the formula for this and other uncommon minerals is given in Table 1). The later and more evolved transsolvus granite contains primary microcline and albite, together with perthite, and the arfvedsonite occurs as phenocrysts. This granite is much more voluminous, and occupies the outer part of the pluton.

The pegmatitic fields, namely, the northwest B-Zone, and the central Main-Zone (Fig. 1), occur mainly as sub-horizontal sheets and lenses ranging from a few cm to 10 m in thickness. The contacts between the pegmatites and granites vary from diffuse to sharp, and locally an aplite layer marks the contact. Mineralogically, the pegmatites are zoned from a border containing coarse-grained euhedral microcline, quartz, arfvedsonite and sodium zircono-(and titano)-silicate minerals to a core dominated by quartz and fluorite with variable proportions of REE and Nb minerals (e.g., bastnäsite-(Ce), fluocerite-(Ce), gadolinite-(Y), allanite-(Ce) and pyrochlore). Both pegmatite fields contain potentially exploitable resources of the REE, Zr and Nb, although only the resource of the B-Zone has been rigorously evaluated. The indicated resources for this zone are 278 Mt of ore, grading 0.94 wt. % REE_2O_3 (38% heavy rare-earth oxides), 1.92 wt. % ZrO_2 and 0.18 wt. % Nb_2O_5. There is also a high-grade spine containing 20 Mt of ore grading 1.44 wt.% REE_2O_3 (50% heavy rare-earth oxides), 2.59 wt. % ZrO_2 and 0.34 wt. % Nb_2O_5 (www.questrareminerals.com).

Evidence of hydrothermal alteration in the pegmatites is widespread. Microcline was albitised, arfvedsonite was altered to aegirine (± hematite), the sodium zirconosilicate (elpidite) was altered to calcium zirconosilicates (gittinsite and armstrongite) and/or zircon, and the sodium titanosilicate (narsarsukite) was replaced by titanite. Finally, phyllic alteration is manifested by

the replacement of primary arfvedsonite and feldspar with Fe- and Al- phyllosilicates (Gysi and Williams-Jones, 2013; Gysi et al., 2016).

A bright purple (due to fluorite) and/or reddish coloured (due to hematite) breccia containing angular fragments (from a few mm to several cm in diameter) of the granite and host rocks (quartz monzonite or quartzofeldspathic and biotite gneisses) in a matrix of fluorite and hematite defines the margins of the pluton. The breccia is barren of REE/HFSE mineralisation, although it has been considered as a resource for fluorine.

Previous work

As mentioned in the Introduction, this paper builds on two earlier publications, i.e., Vasyukova et al. (2016) and Vasyukova and Williams-Jones (2018). The former reports the physico-chemical conditions under which the fluid within the Strange Lake pegmatites evolved, and the latter describes the evolving REE and ligand chemistry of the fluid. In the following paragraphs, we briefly summarise the fluid evolution model proposed in these papers and illustrated in Figure 2 of Vasyukova and Williams-Jones (2018).

The starting point for our model (Stage 1) was the exsolution of a hydrothermal fluid from a pegmatitic melt at a temperature of ~450-500 ºC and a pressure of ~1.1 kbar. This fluid contained immiscible aqueous (25 wt.% NaCl eq.) and gas-rich carbonic (CH_4 + up to 20 mol.% H_2) phases and evolved in a closed system during isobaric cooling. The oxygen fugacity was ~ 5.5 units below the quartz-fayalite-magnetite (QFM) buffer.

During Stage 2a (see Vasyukova et al., 2016, for the stage nomenclature), the fluid cooled to ~ 425 °C, which caused oxidation, i.e., fO_2 increased from ~ 5.5 to ~ 4.8 log units below the QFM buffer, and the fluid became CH_4-dominant (H_2 was consumed to produce H_2O). Salinity remained at nearly the same level (23 wt. % NaCl eq.) and the pH was ≥ 10.1. The fluid during Stages 1 and 2a was close to equilibrium with the minerals that had crystallised and the residual melt, and consequently did not hydrothermally alter the pegmatites. There was light REE (LREE) enrichment of the fluid to ~ 30 times the chondrite value (La), an anomalously low Eu content (2.5 times the chondrite value) and concentration of the middle and heavy REE to ~ 15 times the chondrite values.

Cooling to ~ 360 ºC caused further oxidation (fO_2 ~ 3.5 log units below the QFM buffer; Stage 2b), which triggered alteration of arfvedsonite to aegirine. This alteration buffered fO_2 and

prevented formation of CO_2 from CH_4. Instead, it facilitated oxidative coupling of methane to produce higher order hydrocarbons, the most abundant of them being C_2H_6 and C_3H_8. As a result, the salinity of the fluid decreased from ~23 to ~14 wt.% NaCl eq. and the pH decreased slightly to ≥ 9.7. The REE distribution changed considerably from being LREE-enriched to being slightly depleted in LREE, strongly middle REE (MREE)-enriched (~ 20 times the chondrite value) and HREE-depleted (~5 times the chondrite value for Lu).

Stage 3 began at ~ 300 ºC, when the salinity became insufficient for the alteration of arfvedsonite to aegirine and the system became temporarily unbuffered. As a result, oxygen fugacity increased to 1.3 log units below the QFM buffer, causing the fluid to become CO_2-dominated. The newly formed CO_2 produced a sharp decrease in pH, eventually buffering it to ~ 3. The salinity of the fluid decreased to ~ 4 wt.% NaCl eq. This decrease in pH caused the fluid to attack REE-bearing Na-rich minerals leading to a strong enrichment in the fluid of all the REE (La returned to its initial concentration and the concentration of the HREE reached 70 times the chondrite values). It also lead to the dissolution of fluorite, the solubility of which increases with decreasing pH.

Stage 4 began with the release of CO_2 into the adjacent granite. Oxidation continued (fO_2 ~ 2.5 log units above the QFM buffer) and pH gradually increased due to fluid-rock interaction, which governed evolution of the fluid in the subsequent and final stage (Stage 5); the pH increased to a value of ~ 6 and the salinity increased to ~19 wt.% NaCl eq. This fluid was depleted in the LREE and MREE and strongly enriched in the HREE (the concentrations of Yb and Lu reached values of ~ 240 times the chondrite values).

Samples

The samples on which this study is based are the same as those used in our previous work (Fig. 3 in Vasyukova and Williams-Jones, 2018). These samples, the locations of which are shown in Figure 1, comprise: Sample 16, from a border zone of an unaltered pegmatite containing arfvedsonite, microcline, narsarsukite and quartz with CH_4-H_2-bearing fluid inclusions trapped during Stage 2a; Sample 13, from a pegmatite quartz core, which was weakly altered (arfvedsonite was partially replaced by aegirine, and elpidite was partly replaced by zircon and quartz), and contains CH_4-higher hydrocarbon-bearing fluid inclusions trapped during Stage 2b; Sample 11 from the core of a strongly altered pegmatite, in which arfvedsonite was completely replaced by ferroceladonite, and only locally altered to aegirine, elpidite was replaced by zircon and quartz and the fluid inclusions record the transition from the CH_4-rich Stage 2b to a CO_2-rich

Stage 3 fluid (the latter fluid was initially saturated with nahcolite; nahcolite occurs as a trapped phase in some fluid inclusions, and in others nucleated on cooling or did not form); Sample 7, from the quartz core of a strongly hematised pegmatite, containing fluid inclusions, which characterise Stages 4 and 5; and Sample 2 from a quartz vein that cuts hypersolvus granite and contains fluid inclusions trapped at the end of Stage 3. For additional information on these samples, readers are referred to Vasyukova and Williams-Jones (2018); images illustrating the replacement textures involving the minerals described above are provided in Figure 2 of the current paper.

Methodology

Bulk fluid analysis

Crush-leach

The composition of the bulk fluid in each sample was determined using the crush-leach method described in detail in Vasyukova and Williams-Jones (2018); a pair of crush-leach experiments was performed for each sample (see below). This method was employed to permit analyses for elements present in concentrations below those that can be detected by single inclusion methods, e.g., laser ablation induced coupled plasma mass spectrometry (LA-ICP-MS). Cleaned quartz grains (~ 1.5-2 g per sample), without mineral or melt inclusions and with no minerals attached, were crushed in a leaching solution (3 wt.% HNO_3) spiked with uranium (to avoid adsorption of cations on quartz surfaces). The resulting quartz slurry was filtered, and the solutions analysed with Inductively Coupled Plasma Mass Spectrometry (ICP-MS) for a suite of metals. A second set of samples was prepared with ultrapure water as the leaching solution for the determination of ligand concentrations. These samples were analysed with Ion Chromatography (IC).

Inductively Coupled Plasma Mass Spectrometry

Calibration curves were constructed from seven different standard solutions (500, 100, 20, 5, 1, 0.5 and 0.2 ppb). The samples, sample blanks, standard solutions and solution blanks were analysed by ICP-MS at the Department of Earth and Planetary Sciences, McGill University, with a Thermo Finnigan iCapQ ICP-MS coupled to an auto-sampler. The dwell time for analyses was 10 ms and the number of sweeps was set to 100. The following isotopes were analysed: ^{7}Li, ^{9}Be, ^{11}B, ^{23}Na, ^{39}K, ^{27}Al, ^{31}P, ^{44}Ca, ^{45}Sc, ^{47}Ti, ^{55}Mn, ^{57}Fe, ^{66}Zn, ^{85}Rb, ^{88}Sr, ^{90}Zr, ^{93}Nb, ^{137}Ba, ^{178}Hf, ^{208}Pb and ^{232}Th. All counts per second were converted to concentrations in ppb using the

calibration curves. Concentrations calculated for each element from the signal for the blank solution were treated as the detection limits and are reported in Table 2.

Ion Chromatography (IC)

The ligands, namely fluoride (F^-), chloride (Cl^-) and sulphate (SO_4^{2-}), were analysed by Dr. Dirk Kirste of the Department of Earth Sciences, Simon Fraser University, using a Dionex ICS-3000 SP Ion Chromatograph equipped with an AS22 column and a 500 µl sample loading loop. The detection limits were 5 ppb for F^-, 100 ppb for Cl^- and 20 ppb for SO_4^{2-}.

Data treatment (normalisation)

The concentrations of metals and ligands were normalised using the K concentration in the corresponding solutions (Table 2). The absolute concentrations of the metals in the bulk fluids were calculated by normalising the data in Table 2 to the apparent salinity using the Cl concentrations of fluid inclusions determined microthermometrically by Vasyukova et al. (2016). These concentrations are reported in Table 3.

Mineral analysis

The major and trace element compositions of elpidite (Sample 13), arfvedsonite (Sample 16), early aegirine (Sample 16) and late aegirine-hematite (204705 and BZ10076-11) were measured using an Electron Microprobe (EMP) and LA-ICP-MS at McGill University (Department of Earth and Planetary Sciences). The electron microprobe analyses were performed with a JEOL JXA-8900L, using a beam diameter of 15 µm, a beam current of 20 nA and an accelerating voltage of 15-20 kV. The standards employed in the analyses, the counting times and the detection limits for the different elements are reported in Appendix A.

The LA-ICP-MS analyses were carried out on the same spots that had been analysed using the electron microprobe. These analyses were performed using a NewWave 213 nm Nd-YAG laser-ablation system and a Thermo Finnigan iCapQ ICP-MS. The analyses were conducted with a 10 Hz repetition rate, and a 40 µm beam diameter; the NIST 610 glass was used as an internal standard for Si. Data from the EMP analyses were used to correct the LA-ICP-MS data. The results are reported in Table 4.

Thermodynamic calculations

Thermodynamic calculations were undertaken to model the alteration reactions, and to estimate the pH of the fluid in equilibrium with the different mineral assemblages. The software package HCh (Shvarov, 1999; Shvarov and Bastrakov, 1999) was used for this purpose; the sources of the thermodynamic data for the minerals and gases are listed in Appendix B.

Results

Fluid composition

Pegmatite border (Sample 16)

The fluid from Sample 16 (Table 3) has higher concentrations than the fluid from the other samples for K (5,483 ppm), Be (99 ppm), Al (1546 ppm), Rb (257 ppm), Zr (8.1 ppm) and Pb (624 ppm). Indeed, the Pb concentration is about ten times higher than that of any of the other samples, whereas for the other elements the factor is lower, i.e., from 4 (Be) to 1.4 (Zr). This fluid also contains appreciable B (919 ppm) and Zn (393 ppm); these elements reach their highest concentration in the fluid from Sample 13 (1291 and 423 ppm, respectively). The fluid from Sample 16 is also highly enriched in ligands (anions); it has the highest concentrations of Cl^- (13.9 wt.%), F^- (0.65 wt.%), S (0.25 wt.%, most likely as HS^-) and N (0.31 wt.%, most likely as NH_3). However, there is no evidence of oxidised carbonic species, such as HCO_3^-. Compared to the fluid from the other samples, the fluid from Sample 16 has the lowest concentrations of Li, Mn and Sr, i.e., 29, 3.1 and 4.3 ppm, respectively (the ranges of concentrations for Li, Mn and Sr in the fluid from the other samples are 100-548, 7.4-21 and 14-163 ppm, respectively). This fluid is interpreted to represent the fluid exsolved from the magma prior to alteration, based on the coexistence of melt inclusions with the fluid inclusions (Table 2 in Vasyukova et al., 2016).

Pegmatite core

Sample 13

As mentioned above, the fluid from Sample 13 (Table 3) has the highest concentrations of B (1291 ppm) and Zn (421 ppm) of any of the fluids analysed. It also has very high concentrations of Ti (17 ppm versus 2.3-9.3 ppm in the fluid of the other samples). However, the concentrations of K, Al and Rb are half those of Sample 16. The lowest concentrations (relative to those of the other samples) are for Zr, Nb and Th; the concentration of Nb was below the detection limit and

those of Zr and Th are 1 and 1.8 ppm, respectively. The salinity of Sample 13 is significantly lower than that of Sample 16, thus, the concentration of Cl^- is about two times lower, that of F^- is three times lower and the concentration of N (as NH_3) is 1.5 times lower. The sulphur content is similar to that of Sample 16 (0.21 wt.% in the former and 0.25 wt.% in the latter) and, as is the case for Sample 16, there is no evidence of oxidised carbonic species such as HCO_3^- in the fluid.

Sample 11

Unlike Samples 13 and 16, Sample 11 (Table 3) has an extremely high Ca content, 1.8 wt.% (vs 0.26-0.37 wt.% for samples 13 and 16). This sample also has very high concentrations of Fe (188 ppm), Li (148 ppm), Mn (21 ppm) and Sr (163 ppm) relative to the other samples. Although the concentration of Zr is not as high as that of Sample 16, it is significantly higher than that of Sample 13 (5.8 ppm) and is accompanied by a high Hf content (0.1 ppm). The aluminium concentration is the lowest of all the samples (135 ppm) and the Ti content is very low, i.e., 3.3 ppm, which is five times lower than that in Sample 13. The concentration of sulphur (most likely as SO_4^{2-}) is significantly lower than in Sample 13 (733 ppm vs 0.21 wt.%), and the N (as NO_3^-) content is almost two times lower (0.13 wt.%). Unlike the other anions (Cl^-, S and NO_3^-), the F^- content is higher than that of Sample 13 (0.37 wt.%). The most striking feature of the fluid from Sample 11 is presence of a high concentration of HCO_3^- (6.9 wt.%).

Sample 7

The fluid from Sample 7 (Table 3) has the second highest Ca content (0.8 wt.%) after the fluid from Sample 11, but in contrast it has the second lowest K content (0.13 wt.%). It is also relatively enriched in Fe (208 ppm), Li (352 ppm), Mn (11 ppm) and Sr (128 ppm), and depleted in Be (1.9 ppm), B (94 ppm) and Zr (1.2 ppm). Indeed, the concentrations of Be and B are the lowest of all the samples and that for Zr is the second lowest. The sulphate and nitrate contents are very similar to but slightly higher than those for the fluid in Sample 11 (cf. 733 and 1338 for sulphate and nitrate in Sample 11 versus 990 and 1355 for sulphate and nitrate in Sample 7). However, the fluorine content is the lowest of all the samples (780 ppm). As is the case for the fluid from Samples 16 and 13, there is no evidence of a carbonic species, e.g., HCO_3^-.

Quartz vein (Sample 2)

The fluid in Sample 2 (Table 3) has a very similar trace element composition to that of Sample 11, i.e., it also has high concentrations of Mn (18 ppm), Zr (5.2 ppm) and Hf (0.1 ppm), and a

very low concentration of Ti (2.3 ppm). Like Sample 11, it contains a high concentration of HCO_3^- (2.5 wt.%). In some respects, however, it is compositionally similar to the fluid of Sample 13; with the same Fe content (104 ppm), 100 vs 141 ppm Li, 14 vs 24 ppm Be, 14 vs 35 ppm Sr and 30 vs 23 ppm Pb (Table 3). Unlike the fluid in the other samples, the fluid in Sample 2 has a very high Th concentration (11 ppm), and is depleted in anions, i.e., sulphur species and nitrate (380 and 173 ppm, respectively, which are the lowest for any of the fluids). The fluorine content is also lower than in Samples 11 and 13 (0.13 wt.%). Finally, the fluid in Sample 2 has the lowest K content (only 625 ppm) of any of the samples.

Alteration mineralogy

The earliest evidence of alteration in the pegmatites (Stage 2b) is provided by the replacement of arfvedsonite by aegirine (Fig. 2a). This alteration is interpreted to have been accompanied by the precipitation of fluocerite-(Ce), gadolinite-(Ce), zircon and pyrochlore (Fig. 2a). Alteration of perthite was also early (Stage 2b), and is evident in the replacement of the albite lamellae by microcline (see Fig. 5 in Gysi et al., 2016).

The most obvious evidence of alteration during Stage 3 was the replacement of elpidite by zircon and quartz (Fig. 2b). Elpidite also was replaced by Ca-zirconosilicates (Fig. 2c). Although the relative timing of these two types of replacement cannot be deduced from textural relationships, we interpret the latter replacement to have postdated the crystallisation of zircon. The reason for this was the need for Ca, which we show below was supplied later. The other features of the Stage 3 alteration are the widespread evidence for the replacement of microcline and arfvedsonite by ferroceladonite (Fig. 2d) and the albitisation of microcline, which is manifested by rims of albite on microcline (Fig. 6a in Gysi et al., 2016). Fluorite, which is abundant in the cores of the pegmatites, is interpreted to have dissolved in Stage 3.

The main mineralogical changes during Stage 4 were the precipitation of fluorite, fluocerite-(Ce) and fluorite-fluocerite solid solution (see Fig. 5c in Gysi and Williams-Jones, 2013). Locally, ferroceladonite and bastnäsite-(Ce) were deposited in fractures in elpidite (Fig. 2e). During Stage 5, the principal alteration within the pegmatites was the replacement of arfvedsonite by aegirine and hematite (Fig. 2f; this alteration is also seen in the adjacent granite) and the hematisation of the granite. There was also significant precipitation of ferriallanite-(Ce), which based on textural relationships postdated crystallisation of gittinsite (Fig. 10a in Gysi et al., 2016). Late zircon, which occurs primarily in fine veinlets, also postdated gittinsite crystallisation (Fig. 2c). Ferriallanite-(Ce) precipitation was followed by precipitation of gadolinite-(Y) and, in turn,

gadolinite-(Yb), which are interpreted to have been the last REE minerals to crystallise (Fig. 9b in Gysi et al., 2016).

Discussion

Fluid evolution and alteration/precipitation path

In Vasyukova and Williams-Jones (2018), we reconstructed a physico-chemical alteration/precipitation path for the REE based on the composition of the evolving fluid and the composition of the major rock-forming minerals. Here we build on our earlier study and develop a comprehensive model for the hydrothermal mobilisation of the remaining ore metals and a variety of other elements in the Strange Lake pegmatites and adjacent granites. Each of the stages discussed below is based on the fluid chemistry of a sample described in the section entitled 'Samples', and in Vasyukova et al. (2016).

Stages 2a-2b

As discussed earlier, the fluid released by the pegmatite magma was in equilibrium with the major minerals at a temperature ≥425 ºC and, consequently, did not alter the rock (the pH was high; Fig. 3a, light blue line). This fluid is interpreted to have had a salinity of ~25 wt.% NaCl based on the results of microthermometric analyses of aqueous inclusions in magmatic quartz from the border zone of a pegmatite (Sample 16; Vasyukova et al., 2016). The fluid was also enriched in Be, K, Al, Rb, Zr and Pb (Table 3). Cooling-induced oxidation triggered alteration of arfvedsonite to aegirine (the pH decreased slightly; Fig. 3, dark blue line) following Reaction 1-1 (Table 5) at ~ 360 ºC. This alteration buffered fO_2 (facilitating the formation of higher order hydrocarbons via oxidative coupling of methane; see Vasyukova et al., 2016) and caused changes in the fluid composition. For example, the salinity decreased to half due to the consumption of NaCl and the production of HCl, which we propose was partitioned into the vapour, based on the observation that the log K for Reaction 1-2 (Table 5) is positive for temperatures ≥ 230 ºC. At lower temperature (≤ 230 ºC), the log K is negative, resulting in the production of H^+ and Cl^- and an increase in salinity.

The dissolution and precipitation of minerals during cooling from ~ 425 ºC to ~ 360 ºC was reconstructed using the compositions of Fluids 2a and 2b (Fig. 4a) and the composition of arfvedsonite and aegirine (Fig. 4b). From Figure 4a, it is evident that the transition from Stage 2a to Stage 2b was accompanied by removal of F, Be, Zr, Hf, Nb and Pb from the fluid. Our

previous study (Vasyukova and Williams-Jones, 2018) showed that this stage was also characterised by the removal of the LREE from the fluid. We propose that for the LREE, F, Be, Zr, Hf, Nb and Pb, this occurred in large part because of the precipitation of fluocerite-(Ce) (LREE and F), gadolinite-(Ce) (LREE and Be), zircon (Zr and Hf) and pyrochlore (Nb and Pb). In the case of the LREE, this is supported by the observation that fluocerite-(Ce) was present during the alteration of arfvedsonite to aegirine (Fig. 2a); gadolinite-(Ce) and a LREE-enriched zircon are known to be present in the pegmatites (Gysi et al., 2016), although their place in the paragenesis relative to the alteration of arfvedsonite to aegirine has not been established.

The alteration of arfvedsonite to aegirine released significant F, K, Rb, Li and lesser amounts of Be, Zn, Mn and Sr (Fig. 4b). Although appreciable amounts of F, K and Rb were released from arfvedsonite, there was no enrichment of these elements in the fluid (Fig. 4a), indicating that they were consumed by the precipitation of other minerals. As the addition of K was not accompanied by a corresponding addition of Al, we propose that K (and Rb) were consumed mainly through the replacement of albite lamellae in perthite by microcline (see Fig. 5 in Gysi et al., 2016); the fluorine was consumed by the precipitation of fluocerite-(Ce).

Stage 3

Further cooling to ~310 ºC produced massive oxidation (Vasyukova et al., 2016). This occurred because the salinity of the fluid was insufficient to allow Reaction 1-1 (Table 5) to continue, leaving oxygen fugacity unbuffered, which lead to the conversion of CH_4 to CO_2. The latter was accompanied by a precipitous and very rapid drop in pH, and the precipitation of nahcolite (Fig. 3a, yellow line; Reaction 2-1 in Table 5). At some point, nahcolite began dissolving (Fig. 3a, orange line) as a result of the continued decrease in pH that accompanied the ongoing conversion of CH_4 to CO_2. We propose that this was made possible by the kinetic lag between Reactions 2-1 and 2-2 (Table 5). After the dissolution of nahcolite, the pH of the system was buffered by CO_2 gas at a value of ~ 3 (Fig. 3, red curve). The release of Na^+ that followed the dissolution of nahcolite lead to albitisation, which removed Na^+ from the fluid. This, in turn, was accompanied by the removal of Cl^- as the salinity of the fluid decreased from ~14 wt.% (fluid saturated with nahcolite) to ~ 4 wt.% (fluid saturated with CO_2 gas) (Vasyukova et al., 2016). We propose that Cl^- was removed via the same mechanism as was proposed for Stage 2b, i.e., by preferential partitioning of HCl into the gas (Reaction 1-2 in Table 5).

The fluid from Sample 11, which represents Stage 3, had higher concentrations of most of the elements, including Ca, Sr, Fe, Li, Mn, Zr, Hf, Nb and F, than the fluid of the preceding stage

(Fig. 6a). The reason for this was the highly acidic nature of the Stage 3 fluid, which altered the rock aggressively. As the drop in pH was extremely rapid, this alteration would have involved near synchronous decomposition and precipitation of several minerals under conditions, which were probably far from equilibrium. Two processes that had a major impact on the fluid chemistry and mineralogy were the dissolution and recrystallisation of an early REE-rich fluorite to a REE-poor fluorite. This released Ca, Sr, F and REE to the fluid, which lead to the alteration of narsarsukite to titanite (Reaction 3-1) and the consumption of Ca and LREE (Sr remained in the fluid). It also lead to the alteration of elpidite to zircon (Zircon I in Gysi et al., 2016) (Reaction 3-2) and the incorporation of HREE and F in the latter. In addition, the two reactions (3-1 and 3-2) released minor Zr (and Hf) as $ZrF(OH)_3^\circ$ and $ZrF_2(OH)_2^\circ$ (Migdisov et al., 2011) and Nb as $NbF_2(OH)_3^\circ$ (Timofeev et al., 2015), respectively; the narsarsukite contains ~0.5 wt.% Nb (Table 4).

The preceding reactions were followed by precipitation of bastnäsite-(Ce) in response to the high dissolved CO_2 activity and the increasing F and REE contents of the fluid. One of the results of this precipitation was a considerable increase in the molar Ca/F ratio of the Stage 3 fluid relative to that of the preceding stage (2.3 vs 0.5; Table 3) due to the removal of F. Eventually the Ca activity was high enough to promote widespread conversion of elpidite and zircon to gittinsite and armstrongite. The Ca/F ratio was even higher in Stage 4 (see below) ensuring this alteration continued through Stage 4.

We attribute the high concentrations of Fe, Li and Mn to the alteration of arfvedsonite to ferroceladonite; the arfvedsonite contains ~ 0.3 wt.% Li and ~ 0.5 wt.% Mn (Table 4). Our modelling shows that this alteration began at ~ 290 ºC as a result of Reaction 4-1, which occurred when the K^+ activity of the fluid increased due to the release of K^+ during the albitisation of microcline. The alteration of arfvedsonite continued with Reaction 4-2 (Table 5) when arfvedsonite and microcline reacted directly to produce ferroceladonite (Fig. 2d). This alteration ceased at the end of Stage 4 (Fig. 3, dark green line). The other phyllosilicates, Al- and K-phyllosilicates (see Gysi and Williams-Jones, 2013; Gysi et al., 2016), likely crystallised at the same time as the ferroceladonite.

A feature of the Stage 3 fluid, which distinguishes it from the fluid of the preceding stages, is that it has a relatively flat chondrite-normalised REE profile and is strongly enriched in all the REE (Fig. 5). In our recently published study (Vasyukova and Williams-Jones, 2018), we concluded that, at this stage, the fluid was only enriched in the MREE and that the enrichment in

both the LREE and the HREE was due to the presence of inclusions of the earlier (Group 2a) and later (Groups 4 or 5) fluids in Sample 11. This conclusion, however, is probably incorrect. Instead, we now consider it much more likely that the high total REE content (i.e., the enrichment of the LREE, MREE and HREE) in Sample 11, and its relatively flat chondrite-normalised REE profile reflect the dissolution of fluorite (see above), which has high concentrations of all the REE (Table 4).

A number of elements had lower contents in Fluid 3 than in Fluid 2b, namely Ti, Al, B, Zn, Be, and B (Fig. 6a). Titanium and Al were likely consumed by the alteration of elpidite to zircon (Fig. 6b), although Ti activity would also have been buffered to a low value due to the fact that titanite, which replaced narsarsukite, has much lower solubility than narsarsukite. Boron was most likely consumed by albite, and Zn, Be and Al would have partitioned strongly into the phyllosilicates.

Stage 4

Stage 4 commenced when CO_2 gas-saturated aqueous fluid was released from the pegmatites (at a temperature of ~ 230 °C; Fig. 3a), evidence of which is provided by quartz veins that cut the granites and contain up to 20 mole % of CO_2 in the gas phase of primary fluid inclusions (e.g., Sample 2 in Vasyukova et al., 2016). This fluid reacted with the surrounding granite (see the reaction zone adjacent to the vein in Fig. 3d in Vasyukova and Williams-Jones, 2018), which modified its composition. Locally, it deposited ferroceladonite and bastnäsite-(Ce) in fractures in elpidite (Fig. 2d), which could explain the fact that, compared to the fluid from Sample 11 (Stage 3), it has lower concentrations of Fe, Li, K, Na and F, all of which are present in significant amounts in the ferroceladonite (Table 3; Gysi and Williams-Jones, 2013); the precipitation of bastnäsite-(Ce) is consistent with the low LREE concentration of the fluid from Sample 2. The relatively high concentration in Zr reflects equilibration with vlasovite in the granite (open system), or the pre-release composition of the fluid. Likewise, the low concentrations of Ca and F, could reflect equilibration with fluorite, also in the granite.

Our knowledge of the evolution of the fluid in the pegmatites during Stage 4 (and Stage 5) comes largely from the bulk analysis of the fluid from Sample 7, which contains primary Group 4 inclusions (Stage 4) and secondary Group 5 inclusions (Stage 5), in roughly equal proportions (Vasyukova et al. 2016). Because of this, it is difficult to distinguish the changes that occurred in Stage 4 from those that occurred in Stage 5, simply from the bulk composition. The exception is for the REE. From our previous study (Vasyukova and Williams-Jones, 2018), we know that

462 there was an overall decrease in the concentration of the REE as the fluid evolved from Stage 3
463 to Stage 4, and there was a modest depletion in the LREE (Fig. 5). We also know that Stage 5
464 was marked by a very strong depletion in the LREE and a strong enrichment in the HREE (Fig.
465 5).

466 Most of the elements in Sample 7 have lower concentrations than in Sample 11 (Stage 3) (Table
467 3; Fig. 7a). Calcium shows the largest decrease, from 1.8 wt.% to 0.8 wt.% (Table 3). As the
468 microthermometric data for the Group 5 inclusions (Stage 5) are consistent with NaCl being the
469 only salt present (in many inclusions there was massive dissolution of hydrohalite or melting of
470 ice at a temperature close to the eutectic temperature of -21.2 ºC for the system NaCl-H_2O;
471 Vasyukova et al., 2016) we conclude that almost all the Ca in the bulk fluid was contributed by
472 Group 4 inclusions (Stage 4). Given that Group 4 and 5 inclusions were trapped in roughly equal
473 proportions (see above), it follows that the Ca content of the Stage 4 fluid was ~1.6 wt.%, which
474 is very close to that of the Stage 3 fluid (~1.8 wt.%).

475 We propose that after removal of CO_2 (this was triggered by partitioning of HCl back into the
476 liquid; salting out), fluorite ceased dissolving and fluocerite-(Ce) and fluorite-fluocerite solid
477 solution began precipitating (see Fig. 5c in Gysi and Williams-Jones, 2013) in response to the
478 resulting increase in pH (Migdisov and Williams-Jones, 2014). This precipitation of fluocerite-
479 (Ce) and fluorite-fluocerite solid solution helps explain the increase in the Ca/F ratio from 2.3 in
480 Stage 3 to 4.9 in Stage 4-5 (Sample 7). It also explains the overall decrease in REE concentration
481 and small depletion in the LREE in Stage 4 (Fig. 5).

482 The fluid composition and the alteration/precipitation path in Stage 4 were also controlled by the
483 breakdown of arfvedsonite to ferroceladonite (Fig. 3, dark green line) and by other
484 phyllosilicates (see Gysi and Williams-Jones, 2013; Gysi et al., 2016). As discussed above, this
485 reaction released considerable Li and Mn to the fluid. Most of the Fe (and Mn) was conserved as
486 ferroceladonite and the remaining Fe accumulated in the fluid until oxidation caused
487 precipitation of hematite. It was not possible to constrain the fO_2 path for Stage 4 reliably
488 because there was no gas in the system and no reaction to control fO_2. Consequently, we could
489 not determine the temperature of hematite precipitation. The maximum temperature at which
490 hematite was stable is ~230 ºC, which was evaluated from the intersection of the hematite-
491 magnetite buffer with the unbuffered fO_2 path (dashed light green line in Fig. 3b).

Stage 5

The observation that the fluid inclusions representing Stage 5 are all secondary (Vasyukova et al., 2016) indicates that they were associated with an episode of brittle deformation, which must have occurred before the start of this stage. This episode was likely the collapse of the roof of the Strange Lake pluton during the degassing of the pegmatites, which began with the loss of CO_2 at the end of Stage 3, an interpretation that is supported by the presence of a breccia around the complex. The collapse is interpreted to have been initiated by the decrease in volume that accompanied the transformation of the low density CH_4 gas into a higher density CO_2 gas, together with prolonged isobaric cooling and crystallisation. At 360 ºC, CH_4 has a density of ~0.2 g/cm^3, whereas CO_2 has density ~0.7 g/cm^3, which on cooling to 230 ºC increases to ~0.8 g/cm^3. The gas would therefore have occupied four times less space. The increase in density of the aqueous liquid over this temperature was more modest, from 0.8 to 0.9 g/cm^3 or 15% but would still have contributed significantly to the decrease in volume. Finally, the ongoing crystallisation of the magma, which eventually caused the density to increase from ~2.2 g/cm^3 (the density of a typical rhyolitic lava) to ~2.7 g/cm^3 (the density of granite) or 19%, would also have been an important contributor to the overall volume decrease. We envisage that the collapse was followed by decompression facilitated by the development of conical fractures to the margin of the pluton that provided the conduits for the escape of fluids from the pegmatites.

The alteration during Stage 5 (< 190 ºC) was dominated by the breakdown of arfvedsonite to aegirine and hematite (Fig. 3, dashed brown line), which began at a maximum temperature of ~180 ºC as shown by the intersection of the equilibrium boundary for Reaction 5 with the unbuffered fO_2 path in Figure 3b (dashed brown line in Fig. 3a). This released Fe, K, Rb, Li and F to the fluid (Fig. 7b). Iron was concentrated in the granites through hematisation. As shown in Figure 5, the Stage 5 fluid was characterised by a very strong depletion in the LREE, a modest depletion in the MREE and a strong enrichment in the HREE. We interpret the depletion in the LREE to be due to the precipitation of considerable quantities of ferriallanite-(Ce) at the beginning of Stage 5. Similarly, we interpret the modest depletion in the MREE to reflect the deposition of gadolinite-(Y), which replaced ferriallanite-(Ce). The strong enrichment of the fluid in the HREE, however, implies that there was precipitation of a HREE mineral after entrapment of the Stage 5 fluid. We interpret this mineral to be gadolinite-(Yb) based on the observation that gadolinite-(Yb) replaced gadolinite-(Y). A feature of the zirconium mineralogy in Stage 5 was the return to zircon precipitation after the Ca-zirconosilicate alteration of Stages 3 and 4 (Fig. 2c). We attribute this to the very low Ca activity of the Stage 5 fluid, which has a composition close to the eutectic composition of the system NaCl-H_2O (see above). The final

step in Stage 5 was the precipitation of F and Fe as fluorite and hematite, respectively, to form the cement for the fluorite-hematite breccia that surrounds the pluton (as the Stage 5 fluid was Ca-free, the Ca for the fluorite is interpreted to have been supplied by the adjacent gneisses).

A model for the Strange Lake Hydrothermal System

The results of our previous work (Vasyukova et al., 2016; Vasyukova and Williams-Jones, 2018) and the data presented in this paper on the composition of the evolving fluid have allowed us to reconstruct the precipitation/alteration path for the complex hydrothermal system that operated within the rare metal pegmatites of the Strange Lake pluton. We now know that this fluid evolved mainly within a closed system through cooling-induced oxidation of the gas phase. Methane and H_2 (at >425 ºC, Stage 1) gradually oxidised to CH_4 (at ~ 425 ºC, Stage 2a), then to CH_4 + higher order hydrocarbons (at ~ 310-360 ºC, Stage 2b) and finally to CO_2 (at ≤310 ºC, Stage 3). This oxidation controlled pH and, in turn, the precipitation/alteration path. After initially decreasing gradually from an extraordinarily high value of >10 (Stage 2b), pH dropped precipitously with the oxidation of the CH_4 and higher order hydrocarbons to CO_2, between a temperature of ~ 310 °C and ~ 290 °C (Stage 3), to a value of ~ 3. The intensity of alteration was initially mild and then increased sharply to reach a maximum during Stage 3, due to the very acidic nature of the fluid. At ~230 ºC (the beginning of Stage 4), the CO_2 was released from the system, and the pH of the fluid slowly climbed as fluid-rock interaction continued.

The alteration/precipitation path at Strange Lake was controlled mainly by the interaction of the fluid with four minerals, namely arfvedsonite, elpidite, narsarsukite and fluorite (Fig. 8). Arfvedsonite altered in response to oxidation at both high (~ 370-310 ºC) and low (< 180 ºC) temperature and to acidification of the fluid at temperatures between ~ 290 and 190 ºC, whereas elpidite (~ 290-200 ºC), narsarsukite (~290-260 ºC) and fluorite (~ 290-200 ºC) reacted only in response to the decrease in pH. In Figure 8, we illustrate the evolving pH of the fluid during cooling, and the corresponding changes in the mineralogy of the Strange Lake pegmatites (and adjacent granites) as a result of their interaction with this fluid, i.e., the alteration/precipitation path.

Arfvedsonite began altering to aegirine in Stage 2b at ~ 370 ºC (Fig. 8, dark green line) and released K and F, which lead to K-metasomatism and the precipitation of fluocerite-(Ce), gadolinite-(Ce), pyrochlore and LREE-enriched zircon. This alteration also released MREE to the fluid.

Alteration, as noted above, reached its maximum intensity with the precipitous drop in pH to a value of ~ 3 in Stage 3 (310 to 290 °C). As a result, most elements, notably the HFSE, were at their highest concentrations in the fluid, and, thus, were extremely mobile during this stage. The low pH promoted the solubility of fluorite (Fig. 8, purple line), which was mainly responsible for the massive increase in the concentration of Ca in the fluid. Its dissolution also was responsible for the large increase in the concentration of all the REE. At temperatures between ~290 ºC and ~260 ºC, elpidite reacted to form zircon and quartz (Fig. 8), whereas from ~260 ºC to ~200 ºC it was replaced by Ca-zirconosilicates, i.e., armstrongite and/or gittinsite (Fig. 8). Titanite replaced narsarsukite during the breakdown of elpidite to zircon (Fig. 8, light blue line).

The alteration of arfvedsonite to aegirine terminated at the beginning of Stage 3. When the temperature reached ~ 290 ºC, alteration of arfvedsonite resumed with its replacement by ferroceladonite, and continued to the end of Stage 4 (Fig. 8, medium green line). The latter stage began at 230 ºC, when CO_2 gas escaped from the pegmatites along conical fractures generated as a result of the volume decrease that accompanied the conversion of CH_4 to CO_2, isobaric cooling and the ongoing crystallisation of the intrusion. This lead to an increase in pH, which caused fluorite to cease dissolving and brought about the precipitation of fluocerite-(Ce) and fluorite-fluocerite solid solution. Alteration of arfvedsonite to ferroceladonite mobilised F, Na and Fe^{2+} and provided a sink for trace elements, such as Li, B, Mn and Pb.

In Stage 5, Fe-REE silicates precipitated in the order, ferriallanite-(Ce), gadolinite-(Y) and gadolinite-(Yb). Towards the end of Stage 5, the last residues of fluid left the pegmatites. This high salinity Fe- and F-rich fluid hematised the pegmatites and surrounding granite, and deposited fluorite and hematite, forming the cement to the ring breccia at the margins of the pluton. The main alteration during this stage (≤180 ºC; Fig. 8, light green line) was the replacement of arfvedsonite by aegirine and hematite, which did not cause significant mobilisation of elements, except of F and Fe.

Applicability of the model to other peralkaline systems

The results of this study and those of Vasyukova and Williams-Jones (2018) show that the Strange Lake hydrothermal system was closed from the moment of fluid exsolution until the collapse of the roof of the pluton, which occurred as a result of the volume decrease that accompanied isobaric cooling, oxidation and crystallisation of the pegmatites. This closed hydrothermal system evolved due to cooling-induced oxidation of the gas phase, which drove pH to very low values in response to the conversion of CH_4 to CO_2, and caused intense alteration.

589 The question that we now pose is whether the model developed here is unique to Strange Lake or
590 whether it is also applicable to other peralkaline igneous systems?

591 There are several prerequisites for the above model to be applicable. Firstly, the system should
592 be closed, i.e., the rocks should 'stew in their own juices'. Secondly, the initial fluid should be
593 rich in reduced carbonic gases. Without a carbonic component, an aqueous fluid exsolving in a
594 closed system would not undergo a major change in its chemistry, particularly in its H^+ activity.
595 Consequently, it would never cause the intense alteration and mobilisation described here, unless
596 it entered a different rock with which it was not in equilibrium. If the exsolved fluid contained an
597 oxidised carbonic component, i.e., CO_2, then the initial mineral assemblage would have been in
598 equilibrium with CO_2, and consequently, instead of the primary mineral assemblage being
599 agpaitic (evident by complex zircon- and titano-silicates), it would have been miaskitic
600 (zirconium and titanium would be present as zircon and simple oxides, respectively) and remain
601 relatively stable through the hydrothermal stage. Finally, the exsolved fluid should contain an
602 aqueous component in a proportion sufficient to effect the alteration.

603 The prerequisites discussed above are met by many peralkaline agpaitic complexes, both silica-
604 saturated and -undersaturated (Marks and Markl, 2017). Thus, the model developed for the
605 pegmatites of the Strange Lake pluton should be applicable to other agpaitic intrusions, e.g., the
606 Khibiny and Lovozero complexes (Russia) and Ilímaussaq (Greenland). For all three complexes
607 it has been shown that CH_4 (which was accompanied by minor H_2) was the dominant fluid
608 species during the magmatic stage (e.g., Konnerup-Madsen, 2001; Nivin et al., 2005; Beeskow et
609 al., 2006; Krumrei et al., 2007). During the late-magmatic to hydrothermal stage, the same rocks
610 contained a saline H_2O-NaCl (up to about 30 wt% NaCl equivalent) fluid with a high proportion
611 of CH_4 and traces to percentage levels of higher order hydrocarbons (Konnerup-Madsen, 2001;
612 Krumrei et al., 2007; Graser et al., 2008). On cooling, this fluid would eventually have crossed
613 the $fCH_4 = fCO_2$ boundary unless the fO_2 was buffered to values below this boundary.
614 Importantly, in the case of the Khibiny and Lovozero complexes, the presence of a variety of
615 secondary Na-carbonate and bi-carbonate minerals (Nivin et al., 2005), suggests strongly that
616 oxidation continued to Stage 3 of our model, namely the conversion of the reduced carbonic
617 species to CO_2 and the interaction of the latter with a Na-rich fluid. This fluid would have been
618 acidic and capable of altering complex alkali-Zr-(Ti)-silicates, e.g., eudialyte, elpidite or
619 narsarsukite. Fluorite (if present) would have partly dissolved, supplying Ca to the fluid, which
620 could have triggered alteration involving Na-Ca exchange, e.g., the replacement of Na-

zirconosilicates by Ca(±Na)-zirconosilicates, such as seems to have been the case at Ilímaussaq (Borst et al., 2016).

As peralkaline intrusions differ considerably in their composition and magmatic history, it is unreasonable to expect that they would have undergone the same hydrothermal evolution as Strange Lake. Indeed, the three of the examples cited above are silica-undersaturated, whereas Strange Lake is a granite. Nonetheless, we believe that our model may prove useful in helping researchers to reconstruct the paths of alteration/precipitation in these complex intrusive systems.

Acknowledgments

The research was funded by Quest Rare Minerals Ltd, with a matching NSERC Collaborative Research and Development Grant and a NSERC Discovery Grant. Vincent van Hinsberg, Anna Jung, Isabelle Richer and Lang Shi provided valuable advice on sample preparation and analyses. Dirk Kirste of Simon Fraser University performed the IC analyses. Our student volunteer, Anna Migdisova, helped with the sample preparation. The manuscript benefited from a very thoughtful review by Kathryn Goodenough and the comments of an anonymous Chemical Geology referee.

Figure captions

Figure 1. A geological map of the Strange Lake pluton showing the distribution of the granites, pegmatites and fluorite-hematite breccia and the locations of the samples on which this study was based. The map was taken from Vasyukova and Williams-Jones (2018).

Figure 2. Backscattered scanning electron microscope images depicting textural relationships among selected minerals in the Strange Lake pegmatites and adjacent granites (a) Arfvedsonite partially replaced by aegirine in a pegmatitic segregation within transsolvus granite; fluocerite-(Ce) is present along the replacement boundary (Sample 204705). (b) A fragment of elpidite that has been replaced by zircon and quartz along fractures and at the edge of the crystal in a pegmatite dyke cutting the hypersolvus granite (Sample 13). (c) Elpidite replaced by armstrongite that has been cut by narrow veinlets of zircon. This zircon is not to be confused with the early zircon shown in (b); the zircon veinlets are interpreted to have formed during the late stage alteration of pegmatite as a result of the breakdown of armstrongite (the image is from a sample of a Main-Zone pegmatite cutting dark porphyritic unit). (d) Ferroceladonite after microcline in pegmatite within the hypersolvus granite (Sample 7). (e) Part of a fracture in elpidite filled by bastnäsite-(Ce) and ferroceladonite (Sample 13). (f) Aegirine containing fine-grained hematite (white crystals) after arfvedsonite (Sample 204705). For mineral abbreviations refer to Table 1 and for sample locations refer to Figure 1.

Figure 3. (a) A pH-temperature diagram showing the path that was reconstructed for the fluid that exsolved from the Strange Lake magma (pegmatite). The circled numbers are the sample numbers on which the reconstruction was based. The various coloured lines correspond to reactions, which in most cases were controlled by pH. Light blue identifies the initial fluid (Stage 2a), dark blue represents a stage in which arfvedsonite altered to aegirine (Stage 2b), yellow corresponds to nahcolite precipitation and orange to nahcolite dissolution (Stage 3), red shows where fluorite dissolved (Stage 3), dark green indicates the interval during which arfvedsonite was replaced by ferroceladonite (Stages 3 and 4), light green identifies the conditions during which hematite was stable (Stages 4 and 5) and brown the interval during which arfvedsonite was replaced by aegirine and hematite (Stage 5). The light green and brown lines are dashed because the corresponding pH values are inferred not calculated. The grey dashed lines separate the stability fields of arfvedsonite, aegirine and ferroceladonite and the numbers associated with them refer to reactions listed in Table 5. The vertical arrow pointing to CO_2 indicates the temperature at which CO_2 escaped from the pegmatites and the hydrothermal system changed from closed to open. (b) A fO_2-temperature diagram showing the path reconstructed for the fluid shown in (a) (dark blue curve). The dashed dark blue line indicates the temperature below which fO_2 could not be deduced and was therefore assumed to be constant. Also shown are the stability boundaries for Reactions 1-1 (red) and 5 (green) (Table 5) and the magnetite-hematite buffer (light blue). For mineral abbreviations see Table 1.

Figure 4. (a) A diagram showing elements that were depleted (grey field) or enriched (green field) in the fluid during Stage 2b (Sample 13). The degree of depletion or enrichment was calculated by normalising the composition of the fluid during Stage 2a to that of Stage 2b. The hatched zone shows elements for which, statistically, concentration did not change. b) A diagram showing the effect on the fluid of the alteration of arfvedsonite to aegirine during Stage 2b. To estimate this effect, the composition of arfvedsonite was normalised to that of aegirine. The grey area shows elements added to the rock and the blue area indicates elements released into the fluid; the hatched zone shows elements for which, statistically, concentration did not change. The red star for F indicates that although we know that it was released into the fluid, we could not calculate the amount reliably, because the F content of aegirine is below the detection limit. The element order on the X-axis is major cation (Na to K) followed by minor cation (Fe to Th) and anion (Cl to N).

Figure 5. A diagram showing chondrite-normalised REE profiles for the fluids of the different stages in the evolution of the hydrothermal system based on data presented in Vasyukova et al. (2016); the numbers on the profiles refer to these stages. The solid lines represent the data for Samples 16, 13 and 11, whereas the dashed lines represent theoretical reconstructions based on the data for Sample 7 (see Vasyukova et al., 2016, for further detail). The data for chondrite were taken from McDonough and Sun (1995).

Figure 6. (a) A diagram showing elements that were depleted (grey field) or enriched (green field) in the fluid during Stage 3 (Sample 11). The degree of depletion or enrichment was calculated by normalising the composition of the fluid during Stage 2b to that of Stage 3. For further explanation refer to the caption of Figure 4a. b) A diagram showing the effect on the fluid of the alteration of elpidite to zircon during Stage 3. To estimate this effect, the

composition of elpidite was normalised to that of zircon using compositional data for zircon published by Gysi et al. (2016). For further explanation refer to the caption of Figure 4b.

Figure 7. (a) A diagram showing elements that were depleted (grey field) or enriched (green field) in the fluid during Stages 4-5 (Sample 7). The degree of depletion or enrichment was calculated by normalising the composition of the fluid during Stage 3 to that of Stages 4-5. For further explanation refer to the caption of Figure 4a. b) A diagram showing the the effect on the fluid of the alteration of arfvedsonite to aegirine and hematite during Stages 4-5. To estimate this effect, the composition of arfvedsonite was normalised to that of aegirine/hematite. For further explanation refer to the caption of Figure 4b.

Figure 8. A pH-temperature diagram illustrating the alteration/precipitation path for the fluid that exsolved from the Strange Lake magma (pegmatite). The main processes that controlled the composition of the fluid and the precipitation of new phases, are indicated by colours 1-8 in the legend: 1 - exsolution of a reduced aqueous-carbonic fluid from the magma, 2 - alteration of arfvedsonite to aegirine, 3 - conversion of CH_4 and higher hydrocarbons to CO_2, and saturation of the fluid in nahcolite, and then CO_2, 4 - alteration of arfvedsonite to ferroceladonite, 5 - dissolution of fluorite, 6 - alteration of elpidite to zircon and, in turn, gittinsite, 7 - alteration of narsarsukite to titanite, 8 - alteration of arfvedsonite to aegirine and hematite. The dashed black lines indicate the intervals during which particular minerals precipitated. For the abbreviation of mineral names see Table 1.

References

Beeskow, B., Treloar, P.J., Rankin, A.H., Vennemann, T.W., Spangenberg, J., 2006. A reassessment of models for hydrocarbon generation in the Khibiny nepheline syenite complex, Kola Peninsula, Russia. Lithos, 91(1-4): 1-18.

Borst, A.M. et al., 2016. Zirconosilicates in the kakortokites of the Ilimaussaq complex, South Greenland: Implications for fluid evolution and high-field-strength and rare-earth element mineralization in agpaitic systems. Mineralogical Magazine, 80(1): 5-30.

Graser, G., Potter, J., Kohler, J., Markl, G., 2008. Isotope, major, minor and trace element geochemistry of late-magmatic fluids in the peralkaline llimaussaq intrusion, South Greenland. Lithos, 106(3-4): 207-221.

Gysi, A.P., Williams-Jones, A.E., 2013. Hydrothermal mobilization of pegmatite-hosted REE and Zr at Strange Lake, Canada: A reaction path model. Geochimica et Cosmochimica Acta, 122: 324-352.

Gysi, A.P., Williams-Jones, A.E., Collins, P., 2016. Lithogeochemical vectors for hydrothermal processes in the Strange Lake peralkaline granitic REE-Zr-Nb deposit. Economic Geology, 111: 1241-1276.

Konnerup-Madsen, J., 2001. A review of the composition and evolution of hydrocarbon gases during solidification of the Ilímaussaq alkaline complex, South Greenland. Geology of Greenland Survey Bulletin(190): 159-166.

Krumrei, T.V., Pernicka, E., Kaliwoda, M., Markl, G., 2007. Volatiles in a peralkaline system: Abiogenic hydrocarbons and F-Cl-Br systematics in the naujaite of the Ilimaussaq intrusion, South Greenland. Lithos, 95(3-4): 298-314.

Marks, M.A.W., Markl, G., 2017. A global review on agpaitic rocks. Earth-Science Reviews, 173: 229-258.

Migdisov, A.A., Williams-Jones, A.E., 2014. Hydrothermal transport and deposition of the rare earth elements by fluorine-bearing aqueous liquids. Mineralium Deposita, 49(8): 987-997.

Migdisov, A.A., Williams-Jones, A.E., van Hinsberg, V., Salvi, S., 2011. An experimental study of the solubility of baddeleyite (ZrO_2) in fluoride-bearing solutions at elevated temperature. Geochimica et Cosmochimica Acta, 75(23): 7426-7434.

Miller, R.R., Heaman, L.M., Birkett, T.C., 1997. U-Pb zircon age of the Strange Lake peralkaline complex: Implications for Mesoproterozoic peralkaline magmatism in north-central Labrador. Precambrian Research, 81(1-2): 67-82.

Nassif, J.G., 1993. The Strange Lake peralkaline complex, Quebec-Labrador: The hypersolvus-subsolvus granite transition and feldspar mineralogy, McGill University, Montreal, 104 pp.

Nivin, V.A., Treloar, P.J., Korlopleva, N.G., Ikorsky, S.V., 2005. A review of the occurrence, form and origin of C-bearing species in the Khibiny alkaline igneous complex, Kola Peninsula, NW Russia. Lithos, 85(1-4): 93-112.

Salvi, S., Fontan, F., Monchoux, P., Williams-Jones, A.E., Moine, B., 2000. Hydrothermal mobilization of high field strength elements in alkaline igneous systems: Evidence from the Tamazeght complex (Morocco). Economic Geology and the Bulletin of the Society of Economic Geologists, 95(3): 559-575.

Salvi, S., Williams-Jones, A.E., 1996. The role of hydrothermal processes in concentrating high-field strength elements in the Strange Lake peralkaline complex, northeastern Canada. Geochimica et Cosmochimica Acta, 60(11): 1917-1932.

Salvi, S., Williams-Jones, A.E., 2005. Alkaline granite-syenite hosted deposits. In: Linnen, R.L., Samson, I. (Eds.), Short Course Notes - Geological Association of Canada, pp. 315-341.

766 Salvi, S., Williams-Jones, A.E., 2006. Alteration, HFSE mineralisation and hydrocarbon
767 formation in peralkaline igneous systems: Insights from the Strange Lake Pluton, Canada.
768 Lithos, 91(1-4): 19-34.

769 Shvarov, Y.V., 1999. Algorithmization of the numeric equilibrium modeling of dynamic
770 geochemical processes. Geokhimiya(6): 646-652.

771 Shvarov, Y.V., Bastrakov, E.N., 1999. HCh: a software package for geochemical equilibrium
772 modelling. User's Guide., Record 1999/25. Australian Geological Survey Organisation,
773 Record 1999/25, 61 pp.

774 Siegel, K., Williams-Jones, A.E., van Hinsberg, V.J., 2017. The amphiboles of the REE-rich A-
775 type peralkaline Strange Lake pluton – fingerprints of magma evolution. Lithos, 288-289:
776 156-174.

777 Timofeev, A., Migdisov, A.A., Williams-Jones, A.E., 2015. An experimental study of the
778 solubility and speciation of niobium in fluoride-bearing aqueous solutions at elevated
779 temperature. Geochimica et Cosmochimica Acta, 158: 103-111.

780 Vasyukova, O.V., Williams-Jones, A.E., 2018. Direct measurement of metal concentrations in
781 fluid inclusions, a tale of hydrothermal alteration and REE ore formation from Strange
782 Lake, Canada. Chemical Geology, 483: 385-396.

783 Vasyukova, O.V., Williams-Jones, A.E., Blamey, N.J.F., 2016. Fluid evolution in the Strange
784 Lake granitic pluton, Canada: Implications for HFSE mobilisation. Chemical Geology,
785 444: 83-100.

786

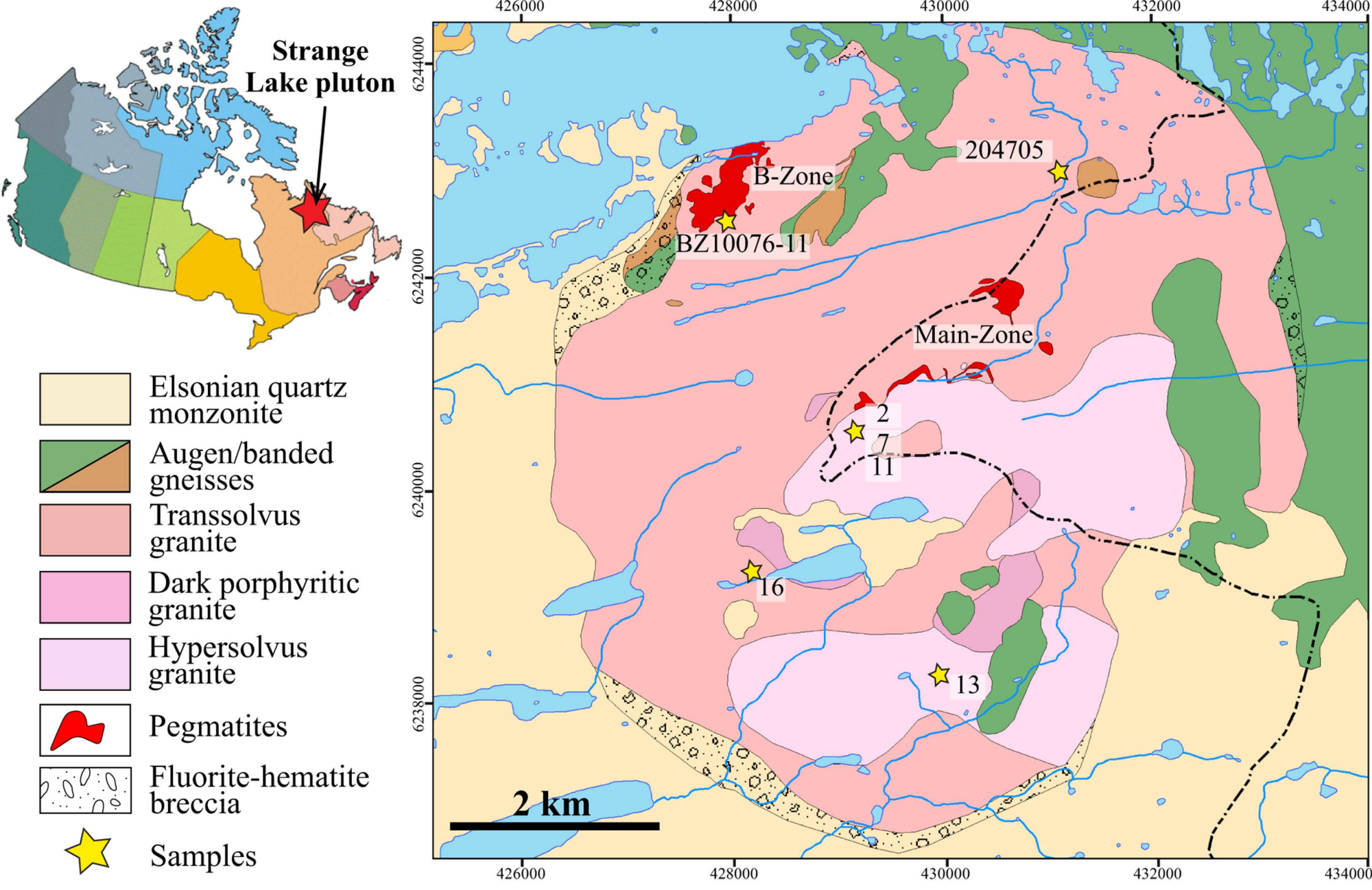
Strange Lake pluton
Elsonian quartz monzonite
Augen/banded gneisses
Transsolvus granite
Dark porphyritic granite
Hypersolvus granite
Pegmatites
Fluorite-hematite breccia
Samples
426000
428000
430000
432000
434000
6244000
6242000
6240000
6238000
B-Zone
BZ10076-11
204705
Main-Zone
2
7
11
16
13
2 km

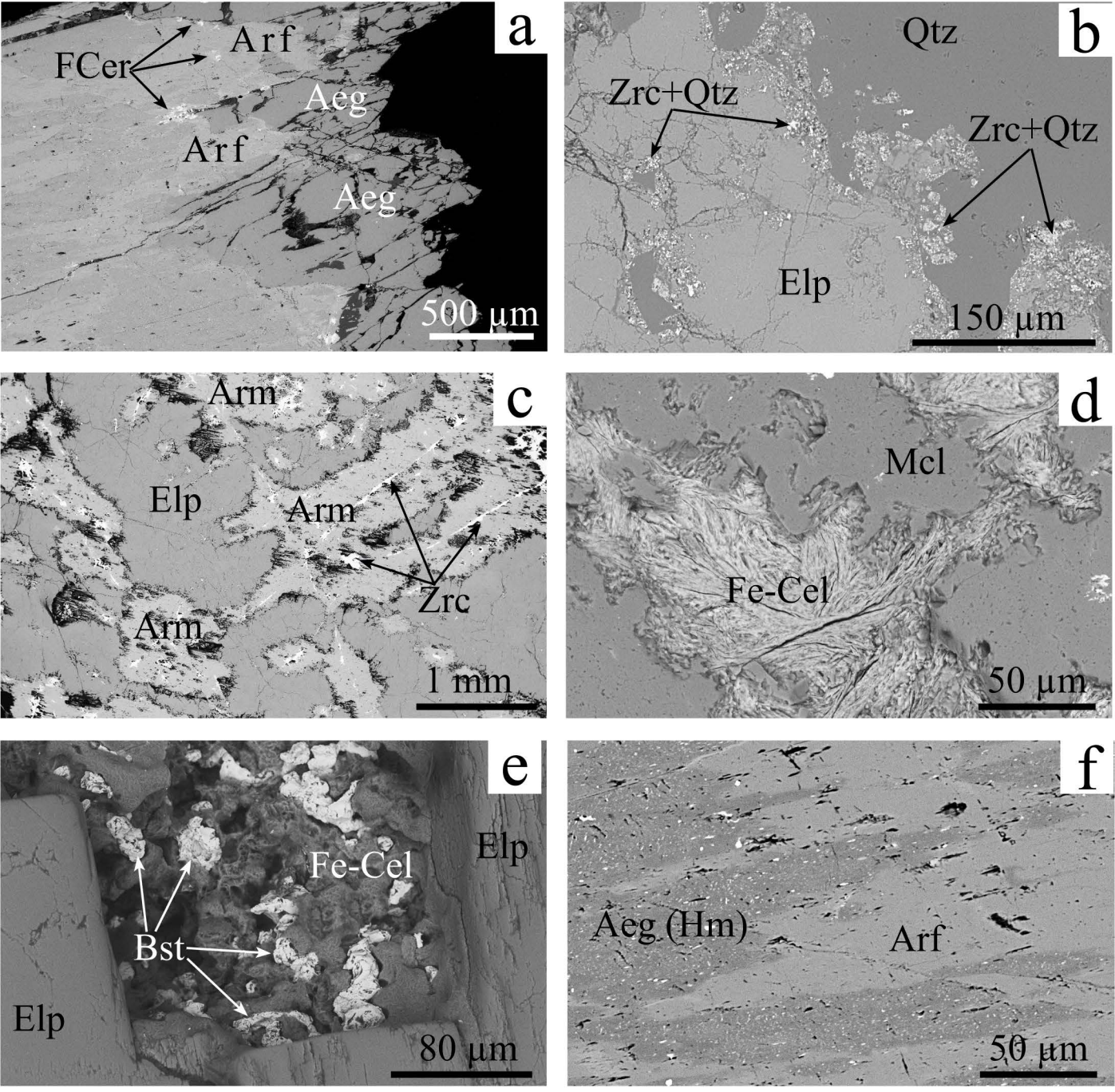
a
FCer
Arf
Aeg
Arf
Aeg
500 µm
b
Qtz
Zrc+Qtz
Zrc+Qtz
Elp
150 µm
c
Arm
Elp
Arm
Zrc
Arm
1 mm
d
Mcl
Fe-Cel
50 µm
e
Fe-Cel
Elp
Bst
Elp
80 µm
f
Aeg (Hm)
Arf
50 µm

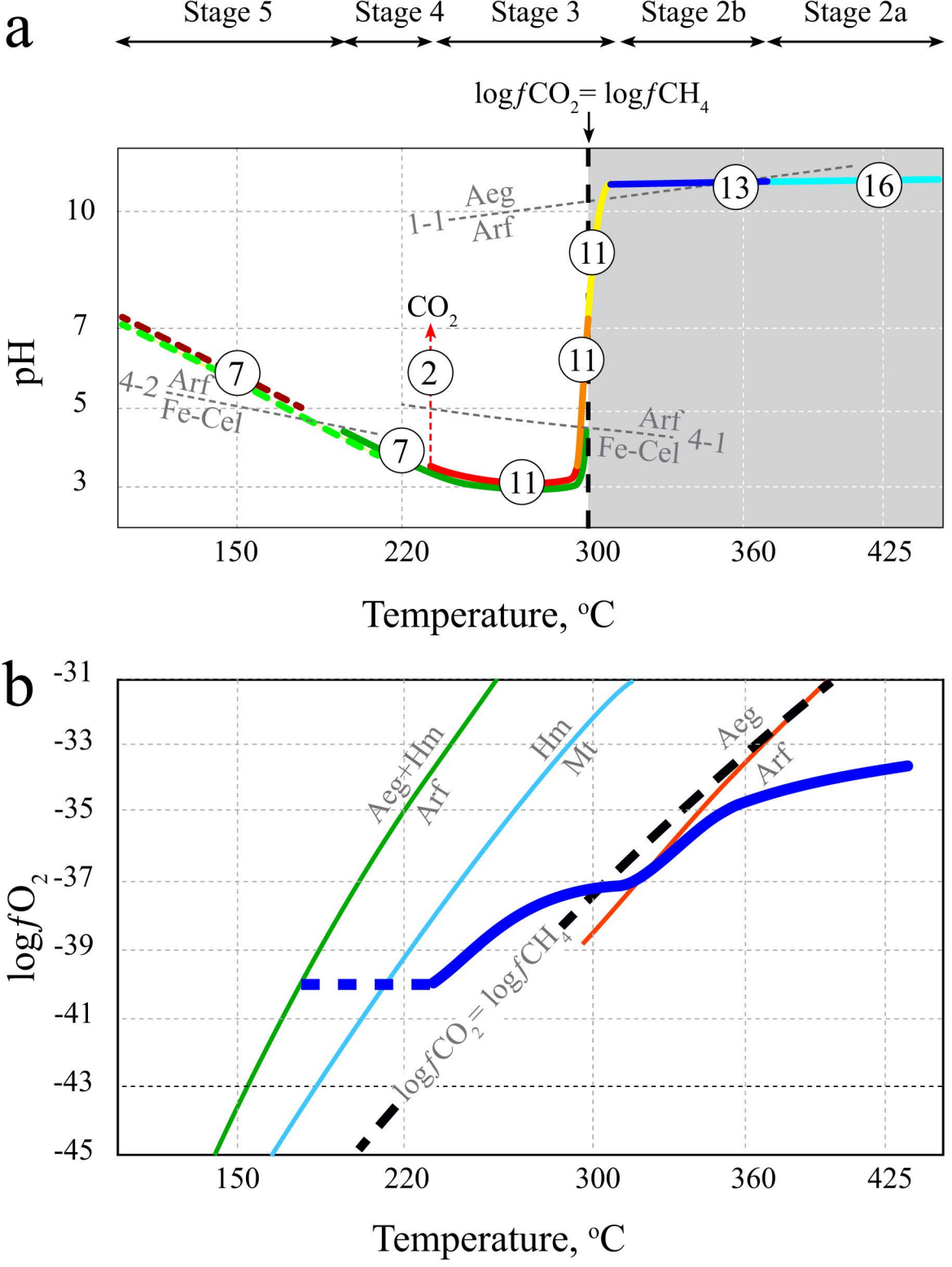
a
Stage 5
Stage 4
Stage 3
Stage 2b
Stage 2a
logfCO2= logfCH4
Aeg
1-1
Arf
13
16
11
CO2
2
11
7
4-2 Arf
Fe-Cel
7
Arf
Fe-Cel 4-1
11
pH
10
7
5
3
150
220
300
360
425
Temperature, °C
b
-31
-33
-35
-37
-39
-41
-43
-45
logfO2
Aeg+Hm
Arf
Hm
Mt
Aeg
Arf
logfCO2 = logfCH4
150
220
300
360
425
Temperature, °C

STAGE 2a → 2b

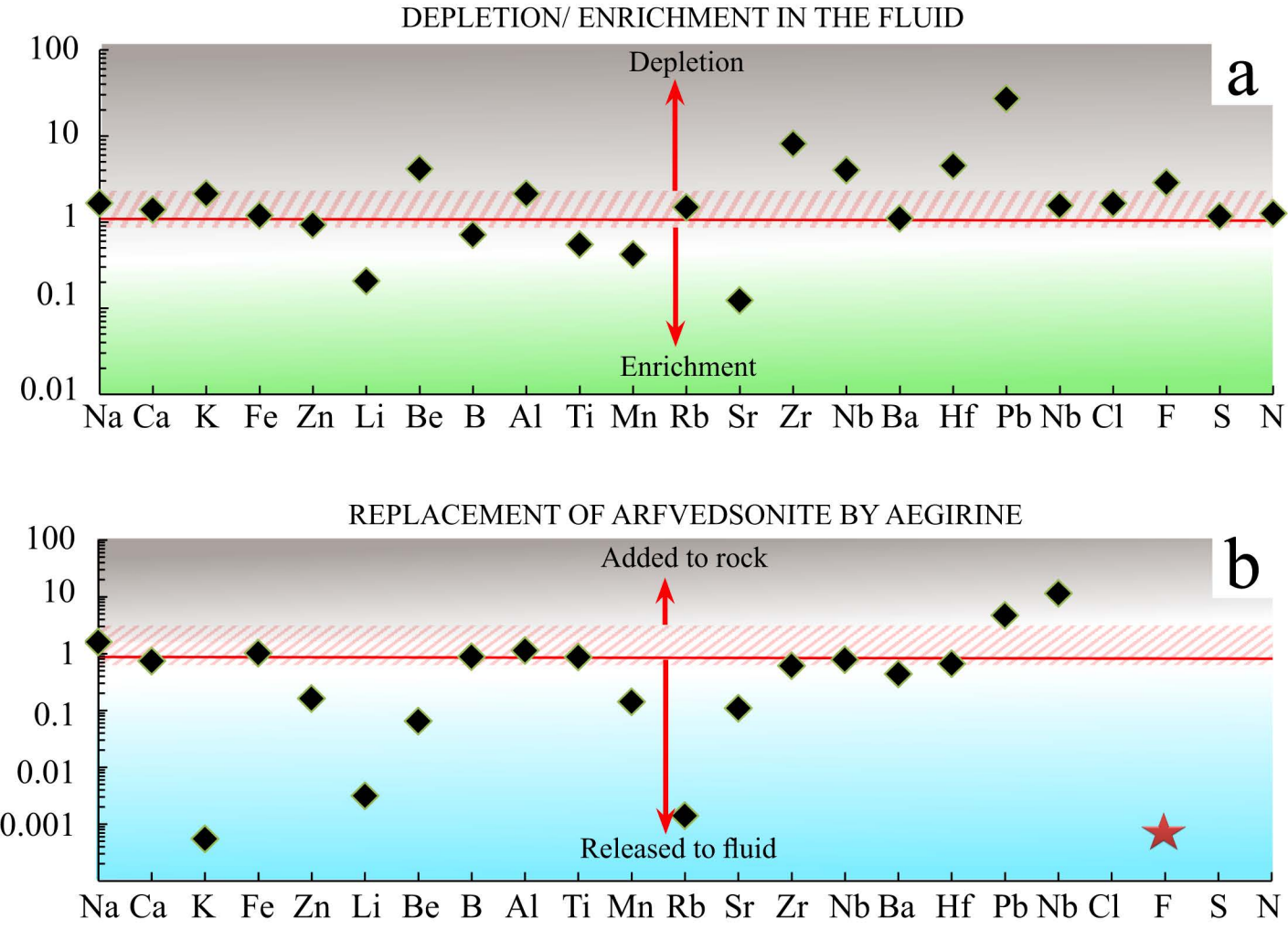
DEPLETION/ ENRICHMENT IN THE FLUID
Depletion
Enrichment
a
100
10
1
0.1
0.01
Na Ca K Fe Zn Li Be B Al Ti Mn Rb Sr Zr Nb Ba Hf Pb Nb Cl F S N
REPLACEMENT OF ARFVEDSONITE BY AEGIRINE
Added to rock
Released to fluid
b
100
10
1
0.1
0.01
0.001
Na Ca K Fe Zn Li Be B Al Ti Mn Rb Sr Zr Nb Ba Hf Pb Nb Cl F S N

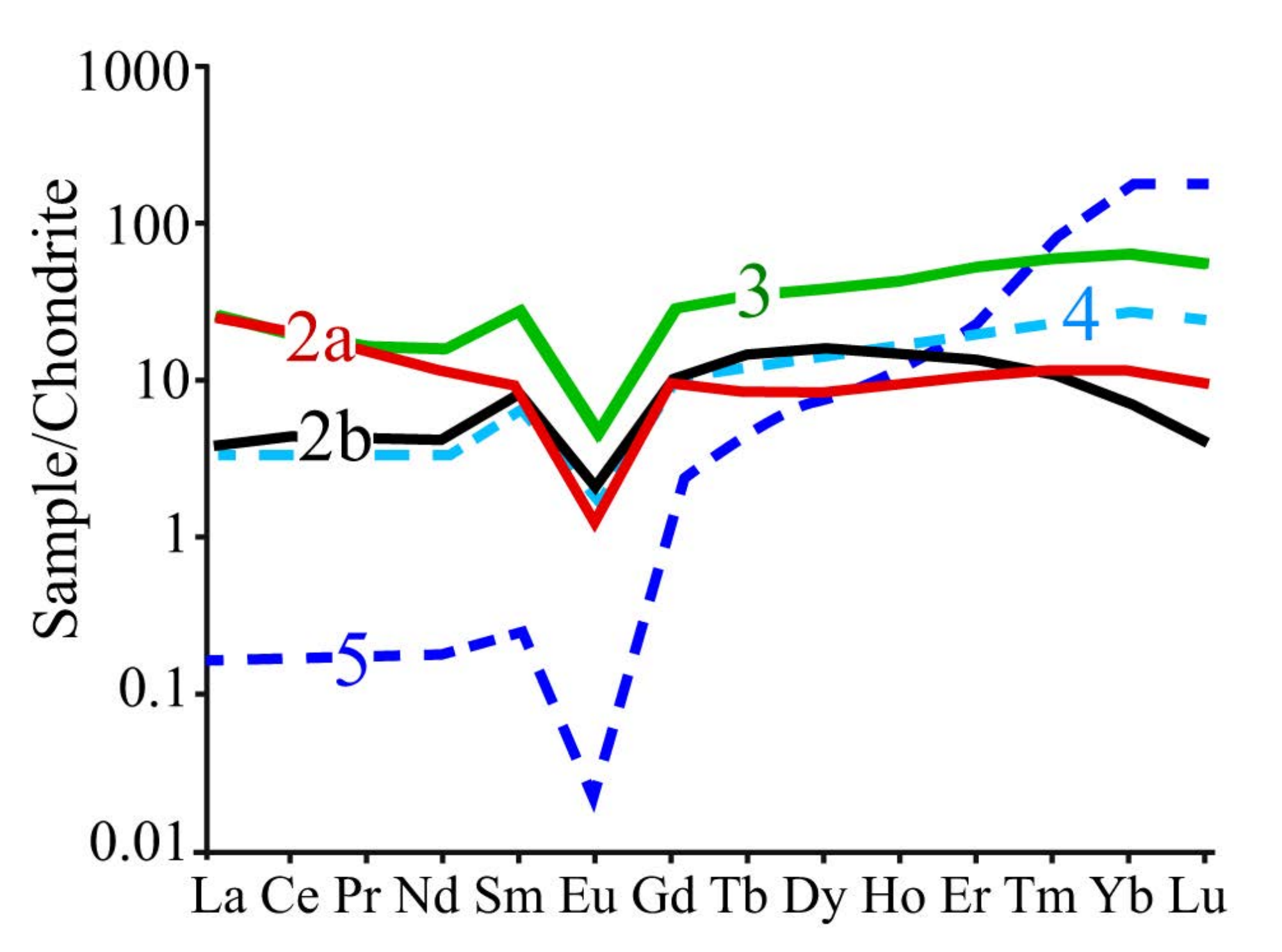
1000
100
10
1
0.1
0.01
Sample/Chondrite
2a
2b
3
4
5
La Ce Pr Nd Sm Eu Gd Tb Dy Ho Er Tm Yb Lu

STAGE 2b ⟶ 3

DEPLETION/ ENRICHMENT IN THE FLUID

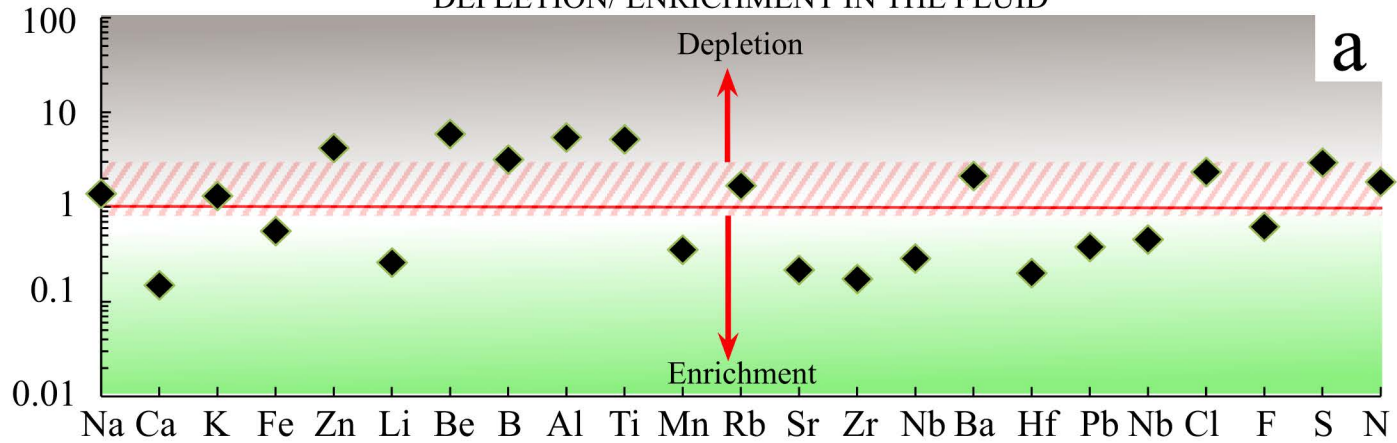

REPLACEMENT OF ELPIDITE BY ZIRCON

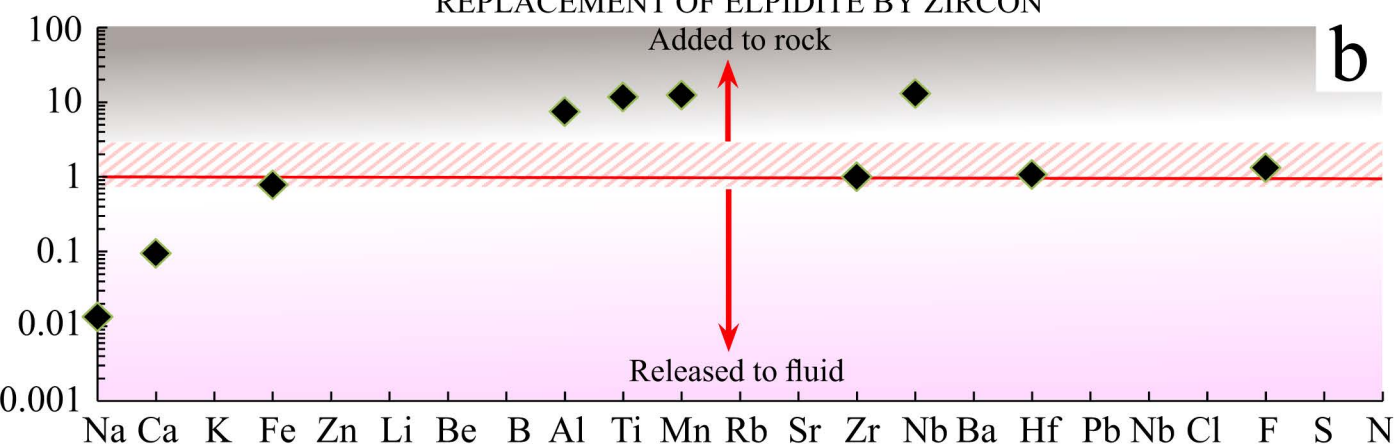

STAGE 3 → 4-5

DEPLETION/ ENRICHMENT IN THE FLUID

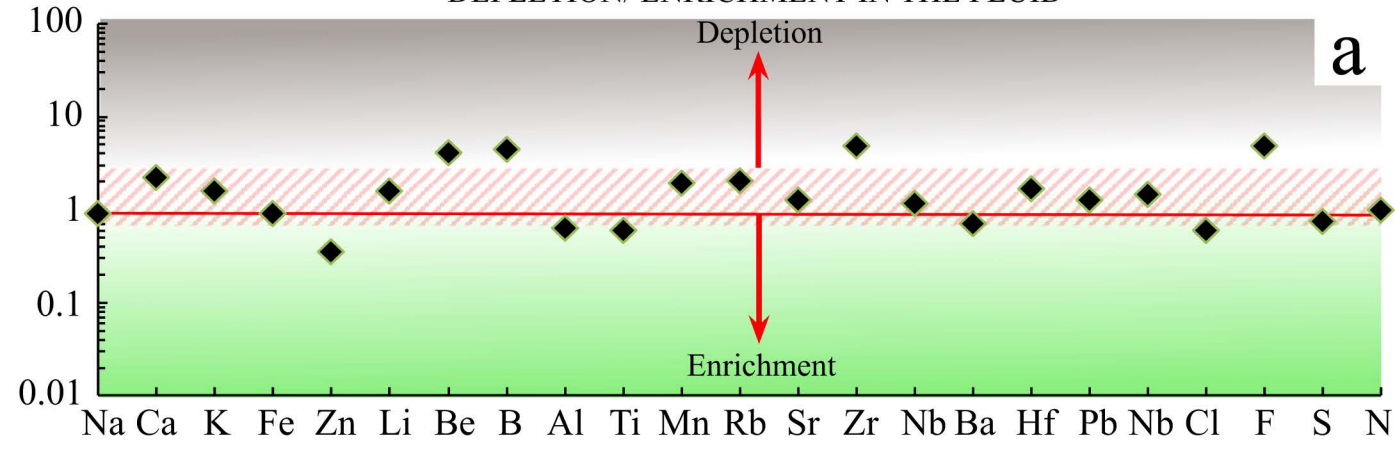

REPLACEMENT OF ARFVEDSONITE BY AEGIRINE AND HEMATITE

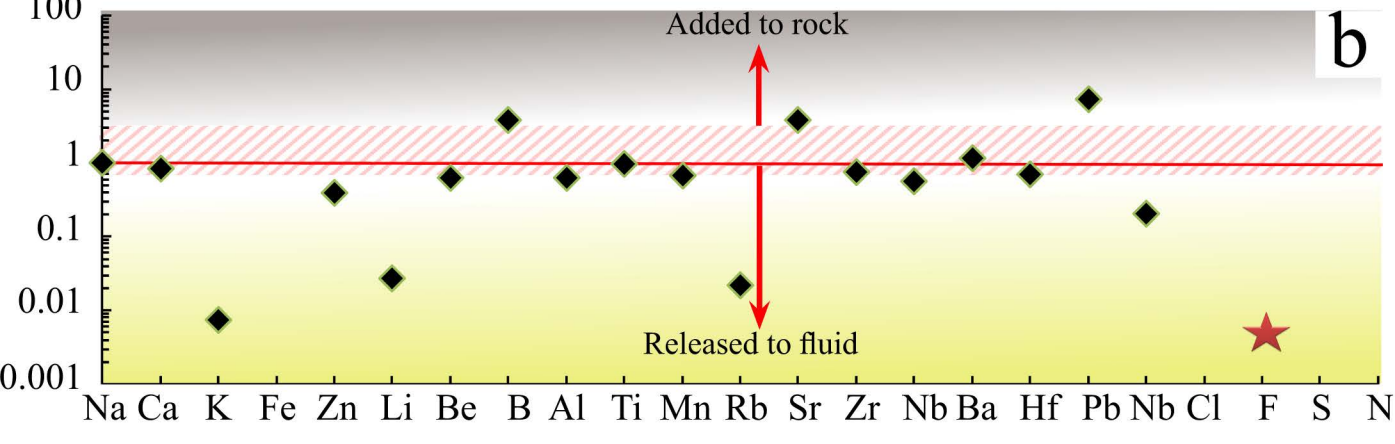

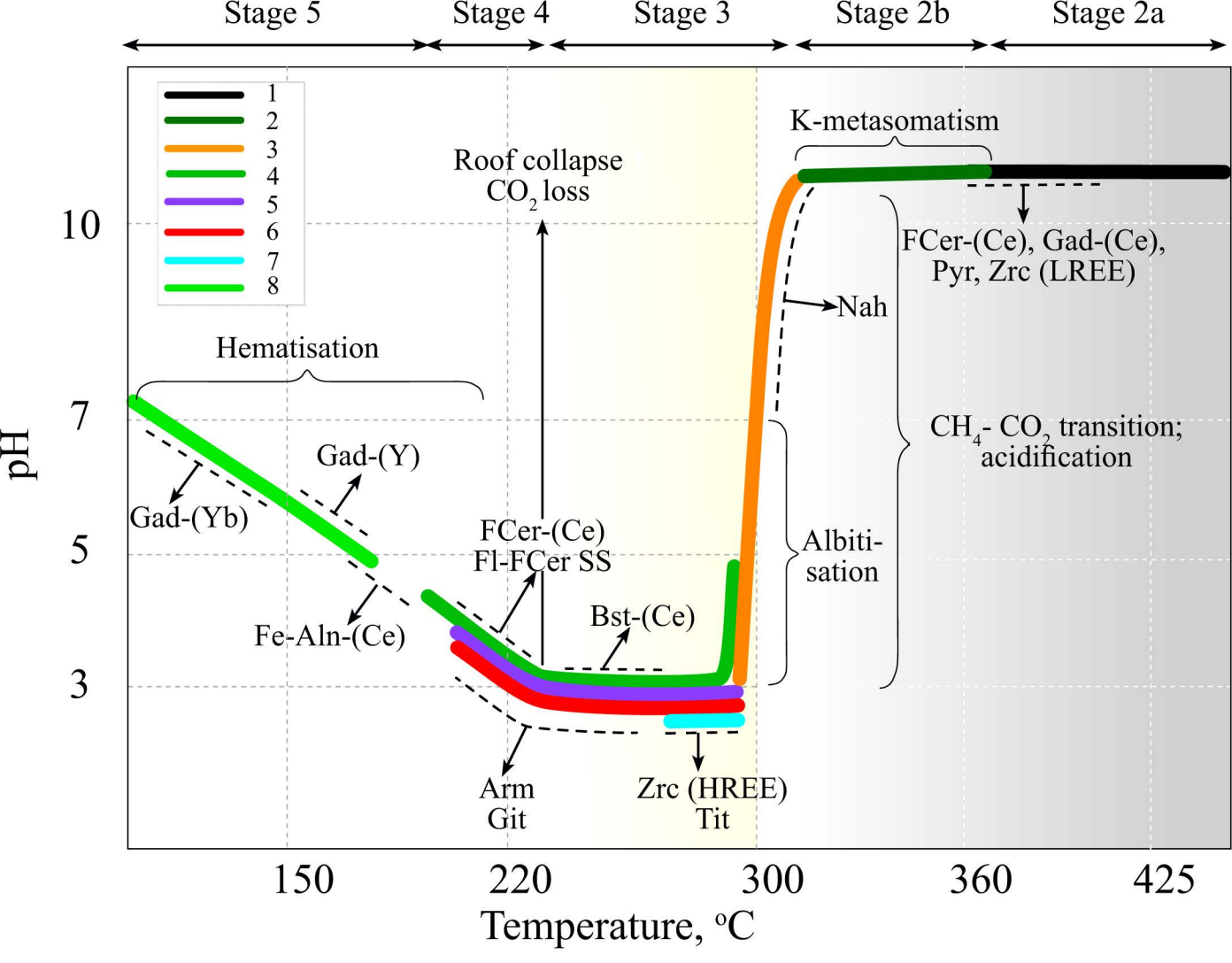
Stage 5
Stage 4
Stage 3
Stage 2b
Stage 2a
1
2
3
4
5
6
7
8
Roof collapse
CO_2 loss
K-metasomatism
FCer-(Ce), Gad-(Ce),
Pyr, Zrc (LREE)
Nah
Hematisation
CH_4- CO_2 transition;
acidification
Albiti-
sation
Gad-(Y)
Gad-(Yb)
FCer-(Ce)
Fl-FCer SS
Bst-(Ce)
Fe-Aln-(Ce)
Arm
Git
Zrc (HREE)
Tit
pH
10
7
5
3
150
220
300
360
425
Temperature, °C

Tables

Table 1. Mineral formulae and abbreviations.

Mineral	Ideal formula	Mineral abbreviations used in Figures
Aegirine	$NaFeSi_2O_6$	Aeg
Albite	$NaAlSi_3O_8$	Alb
Arfvedsonite	$Na_3(Fe^{2+}{}_4Fe^{3+})Si_8O_{22}(OH)_2$	Arf
Armstrongite	$CaZrSi_6O_{15}•3H_2O$	Arm
Bastnäsite-(Ce)	$(Ce,La)(CO_3)F$	Bst-(Ce)
Elpidite	$Na_2ZrSi_6O_{15}•3(H_2O)$	Elp
Ferriallanite-(Ce)	$\{CaCe\}\{Fe^{3+}AlFe^{2+}\}(Si_2O_7)(SiO_4)O(OH)$	Fe-Aln-(Ce)
Ferroceladonite	$K(Fe^{2+},Mg)(Fe^{3+},Al)(Si_4O_{10})(OH)_2$	Fe-Cel
Fluocerite-(Ce)	$(La,Ce)F_3$	FCer-(Ce)
Fluorite	CaF_2	Fl
Gadolinite	$(REE)_2Fe^{++}Be_2Si_2O_{10}$	Gad-(Ce), Gad-(Y), Gad-(Yb)
Gagarinite	$NaCaREE(F,Cl)_6$	Gag-(Ce)
Gerenite-(Y)	$(Ca,Na)_2(REE)_3Si_6O_{18}•2(H_2O)$	Ger-(Y)
Gittinsite	$CaZrSi_2O_7$	Git
Hematite	Fe_2O_3	Hm
Nahcolite	$NaHCO_3$	Nah
Narsarsukite	$Na_2(Ti_xFe^{+++}{}_{1-x})Si_4(O,F)_{11}$	Nar
Magnetite	$Fe^{2+}Fe^{3+}{}_2O_4$	Mt
Microcline	$KAlSi_3O_8$	Mcl
Perthite	$(Na,K)AlSi_3O_8$	Per
Pyrochlore	$(Na,Ca,REE)_2Nb_2O_6(OH,F)$	Pyr
Quartz	SiO_2	Qtz
Vlasovite	$Na_2ZrSi_4O_{11}$	Vls
Zircon	$ZrSiO_4$	Zrc

Table 2. Composition of the leachate fluids (in ppb).

Samples	Blank[1]	PB-1	16	13	11	2	7	PB-2
^{23}Na	**5**	**166**	**2,385**	**3,138**	**5,240**	**8,241**	**2,771**	**39**
^{44}Ca	**9**	**116**	**101**	**158**	**2,434**	**556**	**530**	**103**
^{39}K	**22**	**bdl**	**151**	**155**	**273**	**186**	**82**	**bdl**
^{57}Fe	**3.3**	**12**	**17**	**6.2**	**26**	**31**	**14**	**bdl**
^{7}Li	**0.06**	**0.2**	**0.6**	**8.5**	**75**	**30**	**23**	**0.4**
^{9}Be	0.003	0.02	2.6	1.4	0.6	4	0.06	0.08
^{11}B	1.8	4.9	24	78	56	180	6.1	3.7
^{27}Al	0.4	6.6	20	44	19	75	14	4.5
^{31}P	5.2	10	11	bdl	11	6.5	8.3	bdl
^{47}Ti	0.02	0.3	1.7	1	0.5	0.7	0.4	0.1
^{55}Mn	0.02	0.3	0.5	0.4	2.9	5.5	0.7	0.07
^{66}Zn	0.02	15	14	25	14	19	32	20
^{85}Rb	0.03	bdl	8.2	10	14	24	3.3	0.05
^{88}Sr	0.004	0.4	0.4	2.1	22	4.2	8.4	0.3
^{90}Zr	0.005	0.04	0.2	0.06	0.8	1.5	0.08	0.01
^{93}Nb	0.02	0.05	0.05	bdl	0.1	0.09	0.04	0.02
^{137}Ba	0.004	2	2.3	4.8	5.2	6.5	3.5	4.4
^{178}Hf	0.0002	0.001	0.002	0.001	0.01	0.03	0.004	bdl
^{208}Pb	0.0001	4.4	30	1.4	8.4	8.9	3.2	0.4
^{232}Th	0.0004	0.008	0.06	0.1	0.6	3.2	0.2	bdl
Cl^-	**100**	**bdl**	**3,825**	**5,077**	**4,980**	**7,180**	**3,944**	**bdl**
F^-	**5**	**bdl**	**179**	**137**	**510**	**377**	**51**	**29**
SO_4^{2-}	**20**	**bdl**	**209**	**390**	**306**	**343**	**196**	**84**
NO_3^-	20	52	373	650	815	228	392	294

PB-1and PB-2 – procedure blanks.
bdl – below the detection limit.
The data in bold were reported in Vasyukova and Williams-Jones (2018).
[1] – concentrations in the leaching solution were taken as the detection limits except for F^-, Cl^- and SO_4^{2-} for which detection limits were calculated from IC calibration curves.

Table 3. Composition (in ppm) of the fluids normalised to chlorinity.

Samples	16	13	11	2	7
^{23}Na	**86,556**	**52,208**	**38,092**	**27,705**	**42,391**
^{44}Ca	**3,666**	**2,632**	**17,695**	**1,870**	**8,116**
^{39}K	**5,483**	**2,574**	**1,982**	**625**	**1,259**
^{57}Fe	**124**	**104**	**188**	**104**	**208**
^{7}Li	**29**	**141**	**548**	**100**	**352**
^{9}Be	99	24	4.1	14	1
^{11}B	919	1291	409	604	94
^{24}Mg	67	140	98	39	93
^{27}Al	1546	728	135	252	217
^{47}Ti	9.3	17	3.3	2.3	5.6
^{55}Mn	3.1	7.4	21	18	11
^{66}Zn	393	423	101	109	291
^{85}Rb	257	174	104	79	51
^{88}Sr	4.3	35	163	14	128
^{90}Zr	8.1	1	5.8	5.2	1.2
^{93}Nb	0.8	bdl	0.7	0.3	0.6
^{133}Cs	51	30	13	18	4.2
^{137}Ba	88	79	38	22	54
^{178}Hf	0.09	0.02	0.1	0.1	0.06
^{208}Pb	624	23	60	30	48
^{232}Th	2.8	1.8	4	11	2.8
Cl^-	**138,790**	**84,483**	**36,207**	**24,138**	**60,345**
F^-	**6,509**	**2,274**	**3,704**	**1,267**	**780**
S	**2506**	**2144**	**733**	**380**	**990**
N	3062	2445	1338	173	1355
HCO_3^-	bdl	bdl	69,124*	25,125*	bdl
Charge balance, %	-4.2	-5.4	27.3	17.6	8.4
Molar Ca/F ratio	0.3	0.5	2.3	0.7	4.9

The data in bold were reported in Vasyukova and Williams-Jones (2018)
* - calculated from the charge balance.
bdl – below the detection limit.

Table 4. Major and trace element compositions of selected minerals.

wt%	Elpidite	SD (4)	Arfvedsonite	SD (4)	Aegirine	SD (4)	Aegirine (Hm) 1	SD(10)	Narsarsukite	SD(32)	Fluorite	SD(4)
SiO_2	56.4	0.3	51.6	0.1	53.3	1.2	51.4	0.3	59.9	0.5	0.6	0.5
Al_2O_3	*	*	*	*	*	*	*	*	0.6	0.1	1.0	0.2
TiO_2	*	*	*	*	*	*	*	*	12.6	0.5	2.2	3.1
CaO	*	*	*	*	*	*	*	*	*	*	66.0	4.0
FeO	*	*	31.9	0.8	28.5	0.2	30.0	0.5	4.0	0.8	bdl	bdl
Na_2O	9.1	0.2	9.5	0.1	14.6	0.2	13.0	0.5	15.2	0.3	0.5	0.1
ZrO_2	20.0	0.3	*	*	*	*	*	*	2.0	0.9	bdl	bdl
F	0.2	0.2	2.5	0.2	*	*	0.1	0.2	1.6	0.4	47.0	2.1
Total	85.7		95.6		96.4		94.5		96.0		117.4	
Total[2]	85.6		94.5		96.4		94.4		95.2		94.3	
ppm												
Ca	1,385	53	868	46	695	40	5,514	2,801	1,450	319	**	**
K	177	6.7	15,228	528	3.8	3	102	58	885	255	bdl	bdl
Fe	1,714	144	**	**	**	**	**	**	**	**	bdl	bdl
Zn	2.4	0.4	4,339	178	568	48	6,875	878	88	12	9	6.3
Li	0.6	0.1	3,091	119	7	1.2	49	12	1.2	4.4	bdl	bdl
Be	12	1.1	8	1.4	0.4	0.5	40	18	45	16	bdl	bdl
B	13	0.9	7	1	5.3	1.9	169	74	57	11	bdl	bdl
Al	143	6.4	1,550	50	1,568	133	1,355	131	4,727	580	288	413
Ti	27	1.1	3,146	95	2,678	228	3,081	699	**	**	bdl	bdl
Mn	30	2	5,040	217	623	45	10,552	784	748	90	39	13
Rb	19	0.8	53	1.8	0.05	0.04	2	1.2	5.2	1	1.8	1.2
Sr	74	2.8	0.6	0.05	0.05	0.04	23	13	2.8	0.6	542	148
Zr	**	**	840	35	513	35	1,413	501	**	**	475	158
Nb	83	3.2	95	3.6	69	6.3	227	19	5,133	725	63	20
Ba	33	1.8	0.8	0.1	0.3	0.1	6.9	2.6	0.7	0.7	40	18
Hf	4,133	127	34	1.7	15	1.4	74	41	502	64	13	6.5
Pb	3.4	0.3	13	0.8	80	7.5	1,208	240	13	2.4	44	18
Th	35	2.1	0.4	0.04	4.2	0.4	0.3	0.3	0.02	0.02	15	5.5
La	0.1	0.02	0.8	0.06	4.5	0.6	7.3	2.7	0.04	0.05	3,526	817
Ce	0.7	0.06	2.5	0.1	9.4	0.9	11	4.6	0.6	0.1	4,644	1,290
Pr	0.1	0.01	0.4	0.03	1.1	0.2	1.2	0.4	0.4	0.1	1,021	284
Nd	0.9	0.08	1.7	0.1	5.6	0.3	6.2	2.1	4.4	1.4	7,396	2,064
Sm	0.7	0.07	0.3	0.06	1.1	0.2	1.2	0.4	11	2.2	2,546	787
Eu	1.4	0.1	0.02	0.007	0.07	0.04	0.08	0.02	1.3	0.3	145	55
Gd	1.4	0.09	0.3	0.06	0.8	0.3	1	0.2	50	7.5	2,731	688
Tb	1.3	0.06	0.1	0.01	0.2	0.05	0.4	0.09	38	4.4	385	99
Dy	30	1.2	1.9	0.1	1.3	0.2	5.5	0.8	731	93	2,559	710
Ho	18	0.6	1	0.05	0.3	0.06	2.8	0.5	334	41	462	204

Er	164	6	8.2	0.5	1.6	0.3	19	3.9	1,911	223	1,279	307
Tm	73	2.6	2.8	0.1	0.6	0.08	6.5	1.7	534	58	119	34
Yb	1,039	38	36	1.8	8.7	0.9	76	21	5,162	551	643	252
Lu	146	5.2	7.9	0.4	2.5	0.2	17	5.3	780	87	57	13
Y	292	11	19	0.7	14	1.4	57	11	4,872	754	19,436	4,601
Sc	40	1.2	9.7	0.6	9.8	0.8	12	0.8	25	4.4	bdl	bdl
TREE	1,807		92		61		224		14,453		46,947	

SD (X) - Standard deviation for the number of samples, X.

[1] Aegirine with numerous micro-inclusions of hematite (see text).

[2] Totals corrected for F-oxygen equivalency.

* The value is reported below for the element as a trace element.

** The value is reported above for the element as a major element oxide.

bdl - Below the detection limit.

Table 5. Major reactions controlling composition of the fluid.

#	Reaction
1-1	$Arf + 2\ Qtz + O_2 + 2Na^+ = 5\ Aeg + 2H^+$
1-2	$NaCl° + H^+ = HCl, gas + Na^+$
2-1	$Na^+ + H_2O + CO_2, gas = NaHCO_3 + H^+$
2-2	$CO_2, aq + H_2O = HCO_3^- + H^+$
3-1[a]	$Nar + (x)Ca^{2+} = (x)Tit + (4–x)\ Qtz + 2Na^+ + (1\text{-}x)\ Fe^{3+}$
3-2	$Elp + 2H^+ = Zc + 5\ Qtz + 2Na^+ + 4H_2O$
4-1	$Arf + K^+ + Al^{3+} + 8H^+ = Fe\text{-}Cel + 4Qtz + 4H_2O + 3Na^+ + 3Fe^{2+} + Fe^{3+}$
4-2	$Arf + Microcline + 9H^+ = Fe\text{-}Cel + 7Qtz + 0.5\ Hem + 4.5H_2O + 3Na^+ + 3Fe^{2+}$
5	$Arf + O_2 = 3Aeg + Hem + 2Qtz + H_2O$

[a] – the formula for narsarsukite is $Na_2(Ti_xFe^{+++}_{1-x})Si_4(O,F)_{11}$

Appendices

Appendix A. Standards, counting times and detection limits for EMP analysis.

Element	Standard	Counting time, sec	Detection limits, ppm
Al	Orthoclase	20	211
Ca	Diopside	20	237
F	Fluorite	100	2404
Fe	Hematite	20	270
K	Orthoclase	20	210
Mg	Diopside	20	213
Mn	Spessartine	20	270
Na	Albite	20	252
Si	Diopside	20	356
Ti	Rutile	20	368
Zn	Willemite	20	406
Zr	Zircon	20	821

Appendix B. Sources of data for thermodynamic modelling.

Mineral/aqueous complex	Reference
Aegirine (acmite)	Holland and Powell, 1998
Albite	Holland and Powell, 1998
Arfvedsonite	Calculated; see Vasyukova and Williams-Jones (2018)
Celadonite-Fe	Holland and Powell, 1998
Fluorite	Robie et al., 1978
Hematite	Holland and Powell, 1998
Microcline	Holland and Powell, 1998
Magnetite	Holland and Powell, 1998
Nahcolite	Robie et al., 1978; Vanderzee, 1982
Quartz	Holland and Powell, 1998
CO_2, gas	Holland and Powell, 1998
CO_2, aq	Shvarov, 1999